

AWARD NUMBER: W81XWH-14-1-0218

TITLE: Development of Silicon-Coated Superparamagnetic Iron Oxide Nanoparticles for Targeted Molecular Imaging and Hyperthermic Therapy of Prostate Cancer

PRINCIPAL INVESTIGATOR: Nicholas Whiting, Ph.D.

CONTRACTING ORGANIZATION: The University of Texas MD Anderson Cancer Center  
Houston, TX 77030

REPORT DATE: August 2015

TYPE OF REPORT: Annual Report

PREPARED FOR: U.S. Army Medical Research and Materiel Command  
Fort Detrick, Maryland 21702-5012

DISTRIBUTION STATEMENT: Approved for Public Release;  
Distribution Unlimited

The views, opinions and/or findings contained in this report are those of the author(s) and should not be construed as an official Department of the Army position, policy or decision unless so designated by other documentation.

# REPORT DOCUMENTATION PAGE

*Form Approved*  
OMB No. 0704-0188

Public reporting burden for this collection of information is estimated to average 1 hour per response, including the time for reviewing instructions, searching existing data sources, gathering and maintaining the data needed, and completing and reviewing this collection of information. Send comments regarding this burden estimate or any other aspect of this collection of information, including suggestions for reducing this burden to Department of Defense, Washington Headquarters Services, Directorate for Information Operations and Reports (0704-0188), 1215 Jefferson Davis Highway, Suite 1204, Arlington, VA 22202-4302. Respondents should be aware that notwithstanding any other provision of law, no person shall be subject to any penalty for failing to comply with a collection of information if it does not display a currently valid OMB control number. **PLEASE DO NOT RETURN YOUR FORM TO THE ABOVE ADDRESS.**

<b>1. REPORT DATE:</b> August 2015		<b>2. REPORT TYPE:</b> Annual Report		<b>3. DATES COVERED</b> 15 Jul 2014 - 14 Jul 2015	
<b>4. TITLE AND SUBTITLE</b>  Development of Silicon-Coated Superparamagnetic Iron Oxide Nanoparticles for Targeted Molecular Imaging and Hyperthermic Therapy of Prostate Cancer				<b>5a. CONTRACT NUMBER</b>	
				<b>5b. GRANT NUMBER</b> W81XWH-14-1-0218	
				<b>5c. PROGRAM ELEMENT NUMBER</b>	
<b>6. AUTHOR(S)</b> Nicholas Whiting; Bradley Nolan; Susan Kauzlarich  E-Mail: nwhiting@mdanderson.org				<b>5d. PROJECT NUMBER</b>	
				<b>5e. TASK NUMBER</b>	
				<b>5f. WORK UNIT NUMBER</b>	
<b>7. PERFORMING ORGANIZATION NAME(S) AND ADDRESS(ES)</b>  The University of Texas MD Anderson Cancer Center 1515 Holcombe Blvd Unit 207 Houston TX 77030-4009				<b>8. PERFORMING ORGANIZATION REPORT NUMBER</b>	
<b>9. SPONSORING / MONITORING AGENCY NAME(S) AND ADDRESS(ES)</b>  U.S. Army Medical Research and Materiel Command Fort Detrick, Maryland 21702-5012				<b>10. SPONSOR/MONITOR'S ACRONYM(S)</b>	
<b>12. DISTRIBUTION / AVAILABILITY STATEMENT</b>  Approved for Public Release; Distribution Unlimited				<b>11. SPONSOR/MONITOR'S REPORT NUMBER(S)</b>	
<b>13. SUPPLEMENTARY NOTES</b>					
<b>14. ABSTRACT</b> The main goal of the research project is to develop and test a novel class of dual-threat theranostic nanoparticles for targeted imaging and hyperthermic therapy of prostate cancer. These particles consist of both silicon (for hyperpolarized magnetic resonance imaging, 'MRI') and superparamagnetic iron oxide (for hyperthermic therapy). Preliminary results show that simple mixtures between the two particles still allow for hyperpolarized MRI to take place, albeit with a slightly broadened <sup>29</sup> Si NMR lineshape. The first batch of particles has been completed and physically characterized (tunneling electron microscopy, dispersive x-ray spectroscopy) and shown a viable coupling between the silicon (~300 nm) and iron oxide (~5 nm), with the iron oxide attaching to the surface of the silicon. A small-scale hyperthermia device that induces therapeutic heating in the nanoparticles has been acquired and set up. The next steps include hyperpolarizing this first batch of particles and testing their hyperthermic effect, then applying to gelatin phantoms and prostate cancer mouse models.					
<b>15. SUBJECT TERMS</b> Hyperpolarization, Magnetic Resonance Imaging, Silicon nanoparticles, hyperthermia, superparamagnetic iron oxide nanoparticles, molecular imaging, theranostics					
<b>16. SECURITY CLASSIFICATION OF:</b>			<b>17. LIMITATION OF ABSTRACT</b>  Unclassified	<b>18. NUMBER OF PAGES</b>  36	<b>19a. NAME OF RESPONSIBLE PERSON</b> USAMRMC
<b>a. REPORT</b>  Unclassified	<b>b. ABSTRACT</b>  Unclassified	<b>c. THIS PAGE</b>  Unclassified			<b>19b. TELEPHONE NUMBER</b> (include area code)

## Table of Contents

	<u>Page</u>
<b>1. Introduction.....</b>	<b>4</b>
<b>2. Keywords.....</b>	<b>4</b>
<b>3. Accomplishments.....</b>	<b>4</b>
<b>4. Impact.....</b>	<b>8</b>
<b>5. Changes/Problems.....</b>	<b>9</b>
<b>6. Products.....</b>	<b>10</b>
<b>7. Participants &amp; Other Collaborating Organizations.....</b>	<b>11</b>
<b>8. Special Reporting Requirements.....</b>	<b>11</b>
<b>9. Appendices.....</b>	<b>12</b>

**Department of Defense Congressionally Directed Medical Research Program  
Prostate Cancer Research Program (PCRP)  
Exploration-Hypothesis Development Award W81XWH-13-PCRP-EHDA**

**Title:** Development of Silicon-Coated Superparamagnetic Iron Oxide Nanoparticles for Targeted Molecular Imaging and Hyperthermic Therapy of Prostate Cancer

[PC131680]; W81XWH-14-1-0218

PI: Nicholas Whiting, Ph.D.

**Introduction:** The main goal of this research project is to develop dual-threat nanoparticles that can be used to both detect and treat prostate cancer. To accomplish this, we are developing silicon-based particles that can undergo hyperpolarized (HP) magnetic resonance imaging (MRI) and hyperthermic therapy. Hyperpolarization refers to a collection of methods that can enhance MRI signals by 4-5 orders of magnitude through improved nuclear spin alignment; while this effect typically depletes over the course of one minute, silicon nanoparticles retain their enhanced signal for close to one hour—greatly increasing the window for diagnostic imaging. We are also attaching superparamagnetic iron oxide nanoparticles (SPIONs) to the surface of the silicon particles; when applied with an alternating magnetic field, the SPIONs generate local heating of tumor tissue (~45 °C) without damaging nearby healthy tissue. Hyperthermic therapy has been shown to improve outcomes in resistant tumors when used in conjunction with other chemical and radiation therapies. These particles can also be functionalized with tumor-targeting groups for molecular imaging; in this instance, we plan to target the particles with 7E11-C5.3 antibody, which targets the prostate-specific membrane antigen that is overexpressed in prostate cancer. We plan to develop these targeted particles to be able to (1) image the prostate tumor; (2) undergo hyperthermic therapy; and (3) monitor the efficacy of the therapy in real time. These targeted contrast agents may allow prostate cancer to be detected at an earlier stage; benefits to patients include reduced incidence of invasive biopsies, the ability to monitor therapeutic interventions in real time, and detecting recurrences at lowered thresholds. Therapeutic benefits include enhanced treatment of resistant tumors in combination with chemotherapy or radiation. The objective of this research is to develop hyperpolarized, functionalized Si-coated SPIONs to serve as both a targeted contrast agent for the early detection of prostate cancer, as well as hyperthermic therapy agent. This award should allow the preliminary results needed to acquire additional funding to take this platform to the clinic, where it can directly benefit patients.

**Keywords:** Hyperpolarization, Magnetic Resonance Imaging, Silicon nanoparticles, hyperthermia, superparamagnetic iron oxide nanoparticles, molecular imaging, theranostics

**Accomplishments:**

What were the major goals of the project? The major goals of this project were to: (1) synthesize and characterize SPIONs that contain an outer silicon shell of varying thickness; (2) surface-functionalize the Si-coated SPIONs with murine monoclonal antibody 7E11-C5.3, which has been shown to target prostate-specific membrane antigen—present in ~1,000-fold higher concentration in prostate tumors than normal

tissue; **(3)** determine the extent to which the  $^{29}\text{Si}$  layer can be hyperpolarized using DNP (including polarization level and HP decay time constant); and **(4)** demonstrate viability of generating HP  $^{29}\text{Si}$  MR images, as well as perform hyperthermic treatment, in gelatin phantoms, followed by normal mice and subcutaneous murine cancer models (*LNCaP*).

What was accomplished under these goals? Because of the extended length of time for the awarded institution to get the subcontract with UC Davis activated, the actual project did not start until ~5 months ago. So, we are less than half-way through the initial funding period; because of this, we have applied for (and received) a no-cost extension for a period of 9 months. Thus far, the following activities have taken place:

(1). A hyperthermia device for small animals was acquired from NanoTherics and set-up.



**Fig. 1:** Small-scale hyperthermia device suitable for phantom and rodent studies has been acquired and set up for routine use.

(2). Simple mixtures of silicon particles and SPIONs (with varying concentration of SPIONs) were shown to still produce hyperpolarized  $^{29}\text{Si}$  signal, showing a proof-of-principle that the final particles should also produce hyperpolarized  $^{29}\text{Si}$  signal:

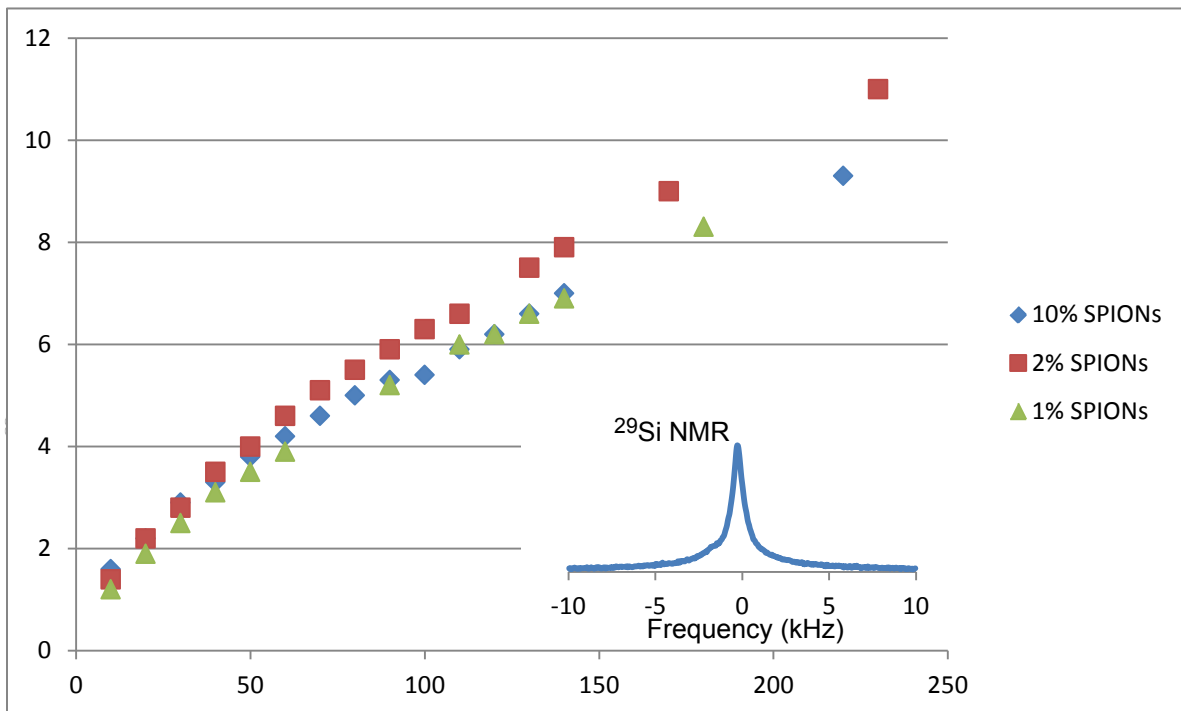
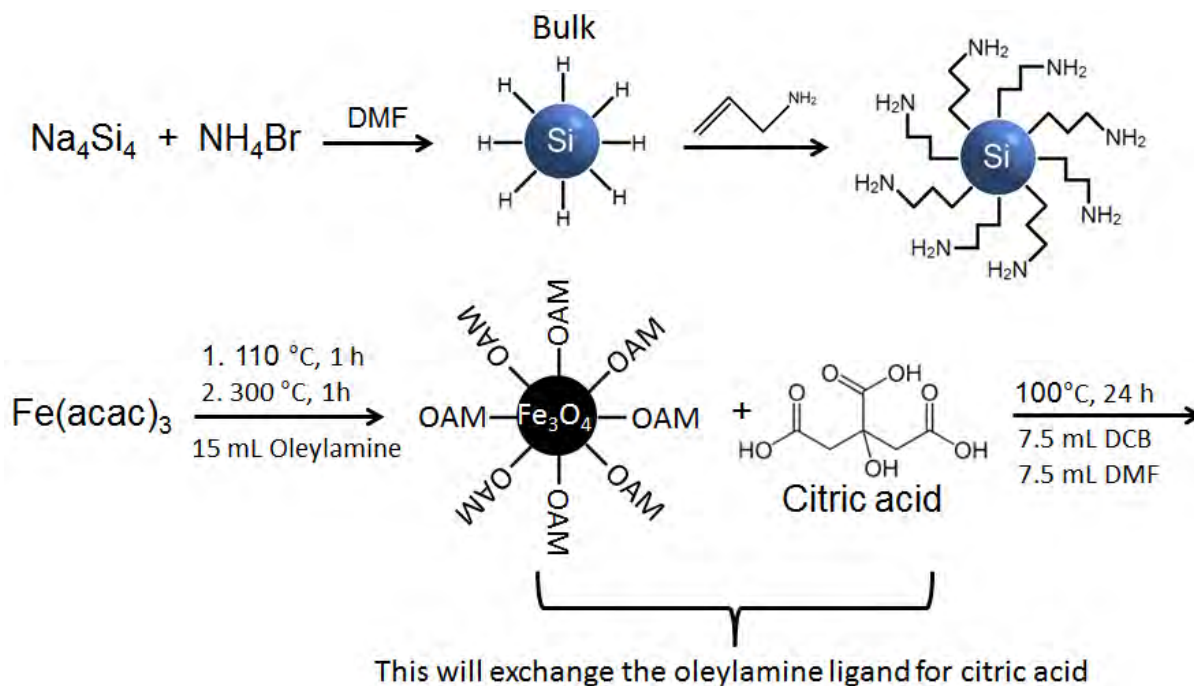


**Fig. 2:** Buildup of  $^{29}\text{Si}$  hyperpolarized MR signal vs. time spent in the DNP polarizer for different mixtures of ~2  $\mu\text{m}$  silicon particles and ~10 nm SPIONs. (*Inset*): Example hyperpolarized  $^{29}\text{Si}$  NMR signal.

The build-up of silicon hyperpolarization over time is quite evident, and the percentage mixture of SPIONs had minimal effect on the hyperpolarization characteristics. Indeed, even the lowest concentration of SPIONs measured here (1%) is at least 10x greater than the actual percentage of SPIONs on the final particles.

(3). A method was devised for creating the silicon/SPION particles



(4). This method was used to create the first batch of SPION-linked silicon particles through the following:  $\text{Na}_4\text{Si}_4$  is combined with  $\text{NH}_4\text{Br}$  to form hydrogen-terminated silicon particles of varying size (few hundred nm). These particles are then further reacted to coat the surface with a reactive amine group. The SPIONs are synthesized using  $\text{Fe}(\text{acac})_3$  at two temperature ranges while exposed to oleylamine; the oleylamine group is then exchanged to form citric acid terminated SPIONs of ~5 nm in size). The SPIONs can then cross-link to the surface of the amine-terminated silicon particles through an EDC coupling (1-ethyl-3-(3-dimethylaminopropyl)carbodiimide).

This reaction has successfully resulted in the creation of silicon particles that are covered in SPIONs. While this is slightly different than the original goal (SPIONs covered in a Si shell), we feel that this direction may be advantageous because: (1) the core Si nuclei should retain their hyperpolarization for longer time periods because they are further away from the SPIONs, which act as a relaxation sink, and (2) the SPIONs will be more capable of producing a hyperthermic heating effect because they won't be insulated by a bulk silicon layer. Thus far, both silicon particles (~300 nm) and SPIONs (~5 nm) have been individually synthesized in the lab, and have now been EDC-coupled:

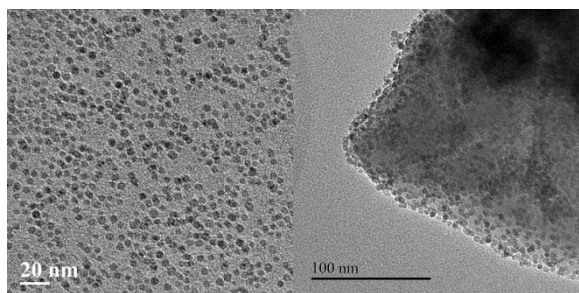
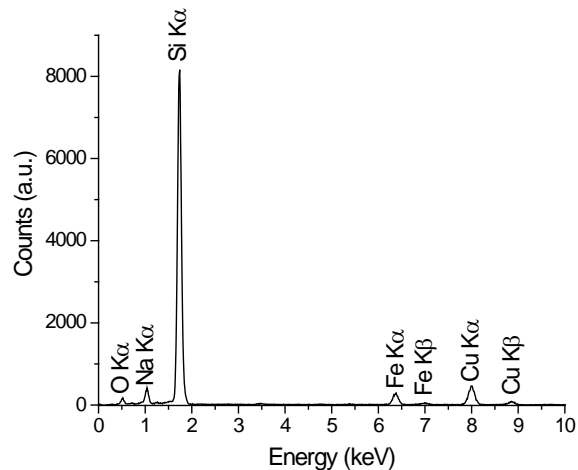


**Fig. 3:** (Left): Individual SPIONs; (Middle): SPIONs dotting the surface of a larger Si particle; (Right): Dispersive X-ray spectroscopy confirming chemical composition of particles



A full image of a Si/SPION particle is shown below:

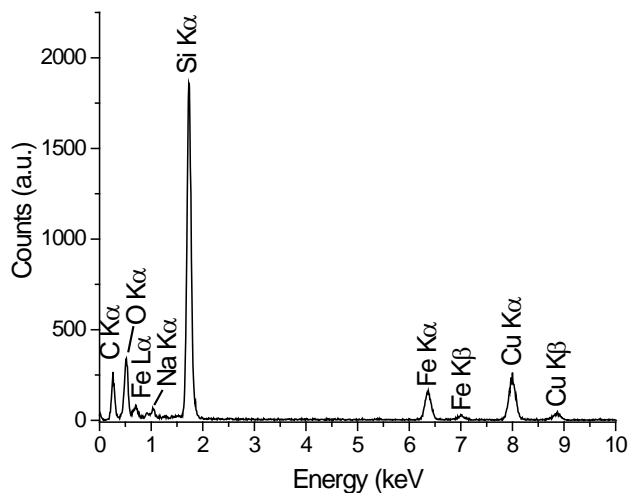
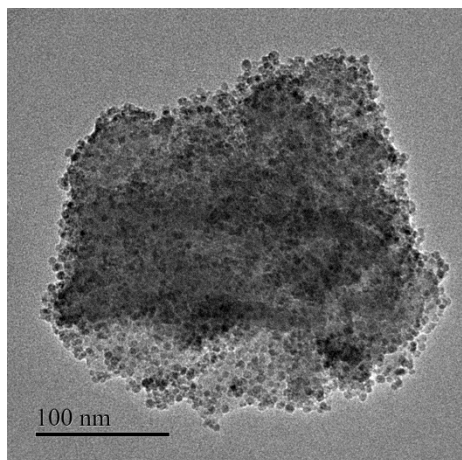


**Fig. 4:** (Left): SPIONs dotting the surface of a larger Si particle; (Right): Dispersive X-ray spectroscopy confirming chemical composition of particles

Thus far, the specific objectives that have been met have been to design and synthesize the Si/SPION particles, which is in line with the predicted timeframe (given the later starting date). The next steps are to observe the hyperpolarization characteristics and hyperthermia effects of these particles.

What opportunities for training and professional development has the project provided? This project has provided numerous opportunities for both training and professional development. This award represents the very first grant for the PI, who is currently a postdoctoral fellow at MD Anderson Cancer Center. This opportunity has given the PI experience in leading all aspects of a project, as well as collaborating with the sub-contracted team that produces the nanoparticles. Money from the grant is supporting both the PI and a graduate student (at UC

Davis); the experience of communicating over long distances and across fields has been helpful for both parties. This has also given the PI excellent experiences in both collaborating and acting as a mentor to a graduate student. During the course of this award, the PI has participated in numerous national/international conferences: International Society of Magnetic Resonance in Medicine; Experimental NMR Conference; Gordon Conference for In Vivo Magnetic Resonance; SPIE: Medical Imaging, as well as many internal talks at the host institution: Odyssey Symposium; Annual Postdoc Science Symposium; Cancer Prevention Research Program 'Brown Bag' Seminars, etc. The PI has also attended several MD Anderson-sponsored career development functions during the award period.

How were the results disseminated to communities of interest? The results of this work have been disseminated at a variety of conferences and invited speaking engagements, including: International Society of Magnetic Resonance in Medicine; Experimental NMR Conference; Gordon Conference for In Vivo Magnetic Resonance; SPIE: Medical Imaging, as well as many internal talks at the host institution: Odyssey Symposium; Annual Postdoc Science Symposium; Cancer Prevention Research Program 'Brown Bag' Seminars, etc. The results have also been discussed at invited lectures at the University of Nottingham and University of York (UK). Preliminary results that apply hyperpolarized silicon particles to MRI-guided catheter tracking were recently published in Scientific Reports, as well as a proceedings paper of the SPIE:

**Whiting, N.,** Hu, J., Shah, J., Cassidy, M.C., Cressman, E., Millward, N.Z., Menter, D.G., Marcus, C.M., Bhattacharya, P.K. *Real-Time MRI-Guided Catheter Tracking Using Hyperpolarized Silicon Particles*. Scientific Reports, **5**, 12842; doi: 10.1038/srep12842 (2015).

**Whiting, N.,** Hu, J., Constantinou, P., Millward, N.Z., Bankson, J., Gorenstein, D., Sood, A., Carson, D., Bhattacharya, P.K. *Developing Hyperpolarized Silicon Particles for Advanced Biomedical Imaging Applications*. Proceedings of SPIE, **9417** (2015).

What do you plan to do during the next reporting period to accomplish the goals? During the next period of time (9-month NCE), we plan to test the ability of these novel particles to hyperpolarize and generate heating upon exposure to an alternating magnetic field. Initial experiments will take place in gelatin phantoms before translating to rodent models of prostate cancer. For these studies, the particles will be functionalized with an antibody to target prostate cancer. Ultimately, we plan to determine whether these particles can be used for dual-purpose, diagnostic and therapeutic studies.

### **Impact:**

What was the impact on the development of the principal disciplines of the project? Thus far, the main impact has been to develop these SPION-functionalized silicon particles, which had not been previously created. Looking forward, if the particles can be shown to be viable for theranostic applications, then they will open a new paradigm where tumors can be interrogated, treated, and the treatment efficacy can be monitored in real time using an imaging modality that is non-invasive and non-radioactive.

What was the impact on other disciplines? Success of this project is also likely to impact other disciplines, including: chemistry & material science (improved synthesis of Si/SPION particles); biomedical imaging & engineering (enhanced non-invasive imaging and targeted therapy); and patient care (reduced need for biopsies and faster determination of treatment efficacy for personalized medicine).

What was the impact on technology transfer? Nothing to report

What was the impact on society beyond science and technology? If successful, this project could result in the preliminary studies of a study that is eventually translated to the clinic, where it will greatly benefit patients.

### **Changes/Problems:**

Changes in approach and reasons for change: Initially, the particles envisioned for this project consisted of a core/shell structure with a SPION core surrounded by a shell (of varying thickness) of elemental silicon. Upon further reflection, we revised the structure of the particle to consist of a large silicon particle that is surface-functionalized with many (hundreds) of individual SPIONs. This was done for three reasons: (1) synthesis of these particles is more straight-forward than the original concept; (2) the new particles should achieve a higher and longer-lasting  $^{29}\text{Si}$  hyperpolarization level and decay time (the particles typically depolarize through spin-diffusion to the surface; the original vision for the particles would add an additional relaxation sink at the center of the particle); and (3) the hyperthermic effect of the SPIONs should be increased due to their closer proximity to the cancer tissue (without being contained inside of a thick layer of insulating silicon). We feel that this second-generation of Si/SPION particles should do a better job of achieving our goal of hyperpolarized imaging and hyperthermic therapy. The only other change was to purchase a commercially-available hyperthermia device instead of assembling one in-house using multiple components. This was done to save time, as we were offered a commercially-available device at a price that was favorable to purchasing the individual components and assembling them (received >50% discount on the device).

Actual or anticipated problems or delays and actions or plans to resolve them: The only delay was an administrative one that took an extended amount of time to get the sub-contract with UC Davis set up. Because the nanoparticles are being synthesized at UC Davis, this delay held up the entire project for over 6 months. We have since gotten the accounts set up and have been approved for a no-cost extension, so we are back on track and do not anticipate any further delays. If it turns out that the Si/SPION particles do not provide sufficient hyperpolarized MRI signal, we will try with just bare silicon particles (as those have also been demonstrated to have a hyperthermic effect).

Changes that had a significant impact on expenditures: The only change in expenditures was purchasing a turn-key solution for the bench-top hyperthermia device instead of making one out of individual components. This was done because the massive discount we received (>50%) made the turn-key solution financially favorable to purchasing individual components. In the end, it didn't cost more to go with this solution (was actually a little cheaper) and saved time in the assembly/testing/optimization of a home-built unit.

Significant changes in use or care of human subjects, vertebrate animals, biohazards, and/or select agents: No changes needed. Have not begun vertebrate animal studies yet. No human studies or use of biohazards anticipated for this project.

## **Products:**

### Publications:

**Whiting, N.**, Hu, J., Shah, J., Cassidy, M.C., Cressman, E., Millward, N.Z., Menter, D.G., Marcus, C.M., Bhattacharya, P.K. *Real-Time MRI-Guided Catheter Tracking Using Hyperpolarized Silicon Particles*. Scientific Reports, **5**, 12842; doi: 10.1038/srep12842 (2015). Published; acknowledged federal support (yes).

### Conference papers:

**Whiting, N.**, Hu, J., Constantinou, P., Millward, N.Z., Bankson, J., Gorenstein, D., Sood, A., Carson, D., Bhattacharya, P.K. *Developing Hyperpolarized Silicon Particles for Advanced Biomedical Imaging Applications*. Proceedings of SPIE, **9417** (2015). Conference proceedings paper; acknowledged federal support (yes).

### Presentations:

**N. Whiting**, J. Hu, N. Millward, R. Rupaimoole, D. Gorenstein, A. Sood, P. Bhattacharya. *Developing Hyperpolarized Silicon Micro and Nanoparticles for Targeted Molecular Imaging of Ovarian Cancer*. 23<sup>rd</sup> International Society of Magnetic Resonance in Medicine, Toronto, Canada, 05/30-06/05, 2015.\*Selected for 1<sup>st</sup> place E-poster presentation in the Molecular & Cellular Imaging Study Group Session.

**J. Hu, N. Whiting**, P. Constantinou, N.Z. Millward, D. Menter, D. Carson, P. Bhattacharya. *Towards Targeted Molecular Imaging of Colorectal Cancer by Hyperpolarized Silicon Particles Functionalized with Mucin Antibody*. 23<sup>rd</sup> International Society of Magnetic Resonance in Medicine, Toronto, Canada, 05/30-06/05, 2015 (Talk).

**N. Whiting**, J. Hu, J. Shaw, M. Cassidy, E. Cressman, C. Marcus, P. Bhattacharya. *Real-Time MRI-Guided Passive Catheter Tracking Using Hyperpolarized Silicon Nanoparticles*. Gordon Research Conference for *In Vivo* Magnetic Resonance, Andover NH, 07/27-08/01, 2014.

**J. Hu, N. Whiting**, J. Shah, N. Millward, M. Cassidy, E. Cressman, C. Marcus, D. Gorenstein, A. Sood, P. Bhattacharya. *Hyperpolarized <sup>29</sup>Si Magnetic Resonance—Towards Applications in MR Guided Catheter Tracking and Targeted Imaging of Cancer*. International Council on Magnetic Resonance in Biological Systems (ICMRBS), Dallas TX, 08/24-29, 2014 (Talk).

**N. Whiting**, J. Hu, M. Cassidy, P.E. Constantinou, N.Z. Millward, D.E. Volk, D.G. Gorenstein, D.D. Carson, C. Marcus, P. Bhattacharya. *Targeted MRI In Vivo by Hyperpolarized Silicon Nanoparticles*. 22<sup>nd</sup> International Society of Magnetic Resonance in Medicine, Milan, Italy, 05/10-16, 2014.

Websites or other Internet sites: None

Technologies or techniques: The technique of attaching SPIONs to silicon particles in this manner is new and will be disseminated with the scientific community through journal articles and conference proceedings. Similarly, using these novel particles for

hyperpolarized imaging and hyperthermic therapy is a new technique that will also be reported through peer-reviewed journals and conference presentations.

Inventions, patent applications, and/or licenses: None

Other products: None

### **Participants and other Collaborating Organizations**

What individuals have worked on the project?

Name:	Nicholas Whiting (UT MD Anderson Cancer Center)
Project Role:	PI
Researcher Identifier:	NWHITING (eCommons name)
Nearest person month worked:	2
Contribution to project:	PI and project lead; oversees all work and corresponds with collaborators; in charge of hyperpolarization and hyperthermic therapy studies; in charge of reporting
Funding support:	

Name:	Bradley Nolan (UC Davis subcontract)
Project Role:	Graduate Student on a Sub-Contract
Researcher Identifier:	
Nearest person month worked:	3
Contribution to project:	Synthesizing Si/SPION particles and performing physical characterization (TEM, XRD, ESR, DLS, etc.)
Funding support:	

Name:	Susan Kauzlarich (UC Davis subcontract)
Project Role:	Professor on a Sub-Contract
Researcher Identifier:	SMKAUZLARAICH (eCommons name)
Nearest person month worked:	1
Contribution to project:	Advising on synthesis routes for the Si/SPION particles
Funding support:	

Has there been a change in the active other support of the PD/PI or senior/key personnel since the last reporting period? Nothing to Report

What other organizations were involved as partners?

Organization Name: University of California Davis

Location of Organization: Davis, California, USA

Partner's contribution to the project: Collaboration; the partner institution was sub-contracted to synthesize and physically characterize the Si/SPION particles.

**Special Reporting Requirements:** None

**Appendices:** Attached (PI's CV; journal article; conference proceeding article; accepted conference abstracts).

# Curriculum Vitae

## Nicholas Whiting, Ph.D.

Odyssey Postdoctoral Fellow  
NCI R25T Postdoctoral Fellow in Cancer Prevention Research  
Department of Cancer Systems Imaging  
The University of Texas MD Anderson Cancer Center

Office: 1881 East Rd  
3SCR4.4803.20; Unit 1907  
Houston, TX 77054  
[nwhiting@mdanderson.org](mailto:nwhiting@mdanderson.org)

### Education

(2005) Bachelor in Science (Chemistry); *Southern Illinois University*, Carbondale, IL

(2010) Doctor of Philosophy (Physical Chemistry); *Southern Illinois University*, Carbondale, IL. Advisor: Prof. Boyd Goodson

### Post-Doctoral Training

(2010-2012) National Science Foundation International Research Fellow; *Sir Peter Mansfield Magnetic Resonance Centre, University of Nottingham*, Nottinghamshire, UK. Advisors: Prof. Peter Morris; Dr. Michael J. Barlow.

(2012-current) National Cancer Institute R25T Postdoctoral Fellow in Cancer Prevention Research and Odyssey Recruitment Postdoctoral Fellow; *Department of Cancer Systems Imaging, The University of Texas MD Anderson Cancer Center*, Houston, TX. Advisor: Prof. Pratip Bhattacharya.

### Honors, Awards, and Fellowships:

Diane Denson Tobola Endowed Fellowship in Ovarian Cancer Research (2015)  
*Magna cum laude* abstract at International Society of Magnetic Resonance in Medicine (2015)  
1<sup>st</sup> Place Electronic Poster Presentation in ISMRM Molecular & Cellular Imaging Study Group (2015)  
MD Anderson Trainee Excellence Award (for professional presentation; 2015)  
Outstanding Postdoctoral Trainee in Cancer Prevention Award (2015)  
MD Anderson Trainee Recognition Award (2014)  
Department of Defense PCRP 'Exploration/Hypothesis Development Award' (detailed below; 2014)  
MD Anderson Odyssey Recruitment Postdoctoral Fellowship (2012-2015)  
NCI R25T Postdoctoral Fellowship in Cancer Prevention Research (2012-2014)  
International Society of Magnetic Resonance in Medicine Educational Stipend Award (2013 & 2015)  
Baxter Young Investigator Award (2012)  
NSF International Research Postdoctoral Fellowship (2010-2012)  
38<sup>th</sup> Southeastern Magnetic Resonance Conference Student Travel Stipend Award (2009)  
Southern Illinois University Dissertation Research Award (2009-2010)  
Robert Gower Summer Research Graduate Fellowship (2009)  
49<sup>th</sup> & 51<sup>st</sup> Experimental NMR Conference Student Travel Stipend Award (2008 & 2010)  
Participant: 57<sup>th</sup> Meeting of Nobel Laureates and Student Researchers, Lindau, Germany (2007)  
C. David Schmulbach Graduate Teaching Assistant Award (2007)  
SIU Dept. of Chemistry Summer Research Undergraduate Fellowship (2004)  
Jim and Jean Neckers Chemistry Scholarship (2004-2005)  
Phi Theta Kappa Honor Society Academic Scholarship (2003-2004)  
Sam Porter Sophomore Chemistry Award (2003)

Peer-Reviewed Publications

Manuscripts Submitted and Currently Under Review:

- (I). ♦ **Whiting, N.**, Newton, H., Morris, P., Goodson, B.M., Barlow, M.J., *Observation of Energy Thermalization and ~1000 K Gas Temperatures during Spin-Exchange Optical Pumping at High Xenon Densities* (manuscript #ANR1059 under revision in Physical Review A; ♦ **corresponding author**).

Published:

- (12). **Whiting, N.**, Hu, J., Shah, J., Cassidy, M.C., Cressman, E., Millward, N.Z., Menter, D.G., Marcus, C.M., Bhattacharya, P.K. *Real-Time MRI-Guided Catheter Tracking Using Hyperpolarized Silicon Particles*. *Scientific Reports*, **5**, 12842; doi: 10.1038/srep12842 (2015).
- (11). **Whiting, N.**, Hu, J., Constantinou, P., Millward, N.Z., Bankson, J., Gorenstein, D., Sood, A., Carson, D., Bhattacharya, P.K. *Developing Hyperpolarized Silicon Particles for Advanced Biomedical Imaging Applications*. *Proceedings of SPIE*, **9417** (2015).
- (10). Nikolaou, P., Coffey, A.M., Walkup, L.L., Gust, B.M., **Whiting, N.**, Newton, H., Muradyan, I., Dabaghyan, M., Ranta, K., Moroz, G.D., Rosen, M.S., Patz, S., Barlow, M.J., Chekmenev, E.Y., Goodson, B.M. *XeNA: An Automated 'Open-Source'  $^{129}\text{Xe}$  Hyperpolarizer for Clinical Use*. *Magnetic Resonance Imaging*, **32**, 541-550 (2014).
- (9). Newton, H., Walkup, L.L., **Whiting, N.**, West, L., Carriere, J., Havermeyer, F., Ho, L., Morris, P., Goodson, B.M., Barlow, M.J., *Comparative Study of in situ  $\text{N}_2$  Rotational Raman Spectroscopy Methods for Probing Energy Thermalisation Processes During Spin-Exchange Optical Pumping*. *Applied Physics B*, **115**, 167-172 (2014).
- (8). Nikolaou, P., Coffey, A., Walkup, L., Gust, B., **Whiting, N.**, Newton, H., Barcus, A., Muradyan, I., Moroz, G.D., Rosen, M., Patz, S., Barlow, M.J., Chekmenev, E., Goodson, B.M., *Near-Unity Nuclear Polarization with an 'Open-Source'  $^{129}\text{Xe}$  Hyperpolarizer for NMR and MRI*. *Proceedings of the National Academy of Sciences, USA* **110**, 14150-14155 (2013).
- (7). \***Whiting, N.**, Nikolaou, P., Eschmann, N., Barlow, M.J., Goodson, B.M., *Frequency-Narrowed, Tunable Laser Diode Arrays with Integrated Volume Holographic Gratings for Use in  $\text{Rb}/^{129}\text{Xe}$  Spin-Exchange Optical Pumping at High In-Cell Xenon Densities*. *Applied Physics B*, **106** (2012) (\*invited paper).
- (6). **Whiting, N.**, Eschmann, N., Barlow, M.J., Goodson, B.M.,  *$^{129}\text{Xe}/\text{Cs}$  ( $D_1$ ,  $D_2$ ) vs  $^{129}\text{Xe}/\text{Rb}$  ( $D_1$ ) Spin Exchange Optical Pumping at High Xenon Densities Using High-Power Broadband Laser Diode Arrays*. *Physical Review A*, **83** (2011).
- (5). **Whiting, N.**, Nikolaou, P., Eschmann, N., Barlow, M.J., Goodson, B.M., *Interdependence of In-Cell Xenon Density and Temperature during  $\text{Rb}/^{129}\text{Xe}$  Spin-Exchange Optical Pumping*. *Journal of Magnetic Resonance*, **208**, 298-304 (2011).
- (4). Barlow, M.J., **Whiting, N.**, Nikolaou, P., Eschmann, N., Mair, R., Goodson, B.M., *A New Spin Exchange Optical Pumping (SEOP) Modality for Hyperpolarized  $^{129}\text{Xe}$  Production and Use in Porous Media*. *Diffusion Fundamentals*, **10**, 116 (2009).
- (3). Nikolaou, P., **Whiting, N.**, Eschmann, N., Chaffee, K.E., Barlow, M.J., Goodson, B.M., *Generation of Laser-Polarized Xenon Using Fiber-Coupled Laser Diode Arrays Narrowed with Integrated Volume Holographic Gratings*. *Journal of Magnetic Resonance*, **197**, 249-254 (2009).

- (2). Saha, I., Nikolaou, P., **Whiting, N.**, Goodson, B.M., *Characterization of Violet Emission from Rb Optical Pumping Cells Used in Laser-Polarized Xe NMR Experiments*. Chemical Physics Letters, **428**, 268-276 (2006).
- (1). Li, X., Newberry, C., Saha, I., Nikolaou, P., **Whiting, N.**, Goodson, B.M., *Interactions Between Xenon and Phospholipid Bicelles Studied by  $^2\text{H}$  /  $^{129}\text{Xe}$  /  $^{131}\text{Xe}$  NMR and Optical Pumping of Nuclear Spins*. Chemical Physics Letters, **419**, 233-239 (2006).

#### Peer-Reviewed Book Chapters

'Spin-Exchange Optical Pumping at High Xenon Densities and Laser Fluxes: Principles and Practice', Goodson, B.M., **Whiting, N.**, Newton, H., Skinner, J.G., Ranta, K., Nikolaou, P., Barlow, M.J., Chekmenev, E.Y. Invited chapter for: Hyperpolarized Xenon-129 Magnetic Resonance (Concepts, Production, Techniques, and Applications). Editors: Meersmann, T., and Brunner, E. Royal Society of Chemistry, UK. (2015).

'Hyperpolarization Methods for MRS'. Goodson, B.M. **Whiting, N.**, Coffey, A.M., Nikolaou, P., Shi, F., Gust, B.M., Gemeinhardt, M.E., Shchepin, R.V., Skinner, J., Birchall, J., Barlow, M.J., Chekmenev, E.Y. Invited chapter for: Handbook of Magnetic Resonance Spectroscopy (MRS); in the Encyclopedia of Magnetic Resonance (eMagRes). Editors: Griffiths, J and Bottomley, P. John Wiley and Sons, Inc. (*in press*).

#### Journal Reviewer

The All Results Journal: Chemistry, Physics, & Nanotechnology (2012-current)

#### Professional Memberships

International Society of Magnetic Resonance in Medicine (*ISMRM*) (2012-current)

National Postdoctoral Association (*NPA*) (2012-current)

#### Additional Activities and Services

Grant reviewer for 'Graduate Technology Enhancement Grant' at SIUC (2010)

Council member for MD Anderson 'Division of Cancer Prevention and Population Sciences Trainee Forum' (2013 & 2015)

Judge for MD Anderson 'Summer Experience Elevator Speech Competition' (2013 & 2014)

Selection committee member for MD Anderson 'Division of Cancer Prevention and Population Sciences Leading Mentor in Cancer Prevention' competition (2013 & 2014)

Finalist (1 of 6) in the MD Anderson Trainee Research Day 'Elevator Speech Competition' (2014)

Finalist (1 of 7) in the MD Anderson Trainee Research Day 'Basic Science Poster Competition' (2015)

Member of MD Anderson Trainee Editing Service Editorial Board (2015)

#### Teaching

Department of Chemistry & Biochemistry, Southern Illinois University, Carbondale IL

(1). CHEM 466A (Thermodynamics Lab, two semesters, ~15-20 students each semester)

(2). CHEM 466B (Quantum Mechanics & Spectroscopy Lab, three semesters, ~15-20 students each)

(3). CHEM 230 (Analytical Chemistry); guest lecturer; ~20-25 students

(4). CHEM 461 (Quantum Mechanics & Spectroscopy); guest lecturer; ~15-20 students

#### Mentoring

1 graduate and 3 undergraduate students in the Dept. of Cancer Systems Imaging, The University of Texas MD Anderson Cancer Center, Houston, TX

2 graduate and 1 undergraduate students at the Sir Peter Mansfield Magnetic Resonance Centre, University of Nottingham, UK

2 graduate and 2 undergraduate students in the Dept. of Chemistry & Biochemistry, Southern Illinois University, Carbondale IL

## Research Support

### Completed

National Science Foundation International Research Fellowship. (PI). 08/2010 – 08/2012. *Fundamental Studies of Spin-Exchange Optical Pumping for the Production of Large Quantities of Highly Spin-Polarized Noble Gases for Improved Magnetic Resonance Applications*. Grant# OISE-0966393. Amount: \$131,420.

### Current

The Applicant is currently supported by a National Cancer Institute R25T Postdoctoral Fellowship in Cancer Prevention Research (R25T CA057730). This award pays 100% of the PI's baseline postdoctoral stipend, plus \$12,625 in research and related expenses per year (~\$130,000 from 2012-2014).

The Applicant is also supported by an Odyssey Recruitment Postdoctoral Fellowship from The University of Texas MD Anderson Cancer Center. This award supplies an additional 20% bonus to the PI's baseline postdoctoral stipend, plus \$5,000 in research expenses per year (~\$50,000 from 2012-2015).

### Recently Approved

Department of Defense Prostate Cancer Research Program Exploration-Hypothesis Development Award. (PI). 07/2014-07/2015. *Development of Silicon-Coated Superparamagnetic Iron Oxide Nanoparticles for Targeted Molecular Imaging and Hyperthermic Therapy of Prostate Cancer*. Amount: \$75,000. (PC131680; funding cut-off line at 5%--double blind review; open to investigators of all ranks).

McCombs Institute Center for Global Cancer Early Detection Award. (Co-Investigator; PI: P.K. Bhattacharya). 08/2015-08/2016. *Non-Invasive Colonoscopy by Targeted Hyperpolarized Molecular Imaging*. Amount: \$200,000.

### Under Review

Department of Defense Lung Cancer Research Program—Concept Award. (PI). 05/2016-05/2017. *Hypoxia-Sensing and pH-Measurement of Lung Tumors using Hyperpolarized <sup>13</sup>CO<sub>2</sub> MRI*. Amount: \$100,000 (under review).

### External Talks:

- (8). **N. Whiting**. *Developing Hyperpolarized Spin Systems for Enhanced Magnetic Resonance Applications*. Centre for Hyperpolarised Magnetic Resonance; Dept. of Chemistry; University of York, UK. 08/07/2015 (*Invited Talk*).
- (7). **N. Whiting**. *Developing Hyperpolarized Spin Systems for Enhanced Magnetic Resonance Applications*. School of Life Sciences, University of Nottingham, UK. 08/05/2015 (*Invited Talk*).
- (6). **N. Whiting**, J. Hu, N. Millward, R. Rupaimoole, D. Gorenstein, A. Sood, P. Bhattacharya. *Developing Hyperpolarized Silicon Micro and Nanoparticles for Targeted Molecular Imaging of Ovarian Cancer*. 23<sup>rd</sup> International Society of Magnetic Resonance in Medicine—Molecular & Cellular Imaging Study Group, Toronto, Canada, 06/04/2015 (*Talk*).
- (5). **N. Whiting**, J. Hu, P. Constantinou, N.Z. Millward, J. Bankson, D. Gorenstein, A. Sood, D. Carson, P.K. Bhattacharya. “*Developing Hyperpolarized Silicon Particles for Advanced Biomedical Imaging Applications*.” Society of Photo-optical Instrumental Engineers Conference (SPIE)—Medical Imaging, Orlando FL, 02/21-26, 2015 (*Talk*).
- (4). **N. Whiting**, J. Hu, J. Shaw, M. Cassidy, E. Cressman, C. Marcus, P. Bhattacharya. “*Real-Time MRI-Guided Catheter Tracking Using Hyperpolarized Silicon Nanoparticles*”. 55<sup>th</sup> Experimental Nuclear Magnetic Resonance Conference, Boston MA, 03/23-28, 2014 (*Talk*).

- (3). **N. Whiting**. “*Fundamental Studies of Spin-Exchange Optical Pumping for the Production of Large Quantities of Highly Spin-Polarized  $^{129}\text{Xe}$  for Improved Magnetic Resonance Applications*”. Baxter Healthcare. Chicago, IL; Sept. 13, 2012 (*Invited talk*).
- (2). **N. Whiting**, P. Nikolaou, N. Eschmann, M. J. Barlow, B. M. Goodson. “*Improved Production of Large Quantities of Highly Spin-Polarized Xenon for Use in Magnetic Resonance Applications*.” 38th Southeastern Magnetic Resonance Conference (SEMRC). Vanderbilt University, Nashville, TN; Nov. 6-8, 2009 (*Talk*).
- (1). **N. Whiting**, P. Nikolaou, N. Eschmann, M. J. Barlow, B. M. Goodson. “*Anomalous High Xenon Polarization at High Xenon Densities Achieved via Optical Pumping with Volume Holographic Grating (VHG)-Narrowed Laser Diode Arrays*.” Chicago Area Nuclear Magnetic Resonance Discussion Group (CANMRDG). Washington University, St. Louis, MO; Nov. 8, 2008 (*Talk*).

Internal Talks (at host institution):

- (10). **N. Whiting**. “*Towards Targeted Molecular Imaging of Different Cancer Systems using Hyperpolarized Silicon Particles*”. MDACC Annual Postdoctoral Science Symposium, Houston TX, 09/17/2015 (*Talk; abstract accepted*)
- (9). **N. Whiting**. “*Hyperpolarized Silicon Particles: Towards Enhanced Targeted Molecular Imaging*”. Odyssey Annual Mini Symposium. The University of Texas MD Anderson Cancer Center. Houston, TX 06/22/15 (*Invited Talk*)
- (8). **N. Whiting**. “*Developing Hyperpolarized Silicon Particles for Targeted Molecular Imaging and Early Detection*.” MDACC Cancer Prevention Research Training Program Trainee Brown Bag Seminar, Houston, TX 03/19/2015 (*Talk*).
- (7). **N. Whiting**, J. Hu, J. Shaw, M. Cassidy, E. Cressman, C. Marcus, P. Bhattacharya. “*Real-Time MRI-Guided Passive Catheter Tracking Using Hyperpolarized Silicon Nanoparticles*.” MDACC Annual Postdoctoral Science Symposium, Houston TX, 08/07/2014 (*Talk*).
- (6). **N. Whiting** & P. Bhattacharya. “*Theranostic Applications of Hyperpolarized Silicon Nanoparticles*.” Texas Center for Nanomedicine meeting, Houston, TX 07/25/2014 (*Talk*).
- (5). **N. Whiting**, P. Bhattacharya, A. Sood, D. Gorenstein. “*Hyperpolarized Silicon Nanoparticles as MR Biomarkers for Early Detection of Ovarian Cancer*.” NCI Alliance for Nanotechnology in Cancer Site Visit. Houston, TX 05/14/2014 (*Talk*).
- (4). **N. Whiting**. “*Implementing Hyperpolarized Silicon Nanoparticles for Biomedical Imaging: MRI-Guided Catheter Tracking and Molecular Imaging Agents for Early Cancer Detection*”. MDACC Cancer Prevention Research Training Program Trainee Brown Bag Seminar, Houston, TX 04/10/2014 (*Talk*).
- (3). **N. Whiting**. “*Towards the Implementation of Hyperpolarized, Functionalized Silicon Nanoparticles as In Vivo Molecular Imaging Agents for the Early Detection of Cancer by Magnetic Resonance Imaging*”. Odyssey Annual Mini Symposium. The University of Texas MD Anderson Cancer Center, Houston, TX, 06/13/2013 (*Invited talk*).
- (2). **N. Whiting**. “*Fundamental Studies of Spin-Exchange Optical Pumping for the Production of Large Quantities of Highly Spin-Polarized  $^{129}\text{Xe}$  for Improved Magnetic Resonance Applications*.” The University of Texas MD Anderson Cancer Center. 7/19/2012 (*Invited Talk*).
- (1). **N. Whiting**. “*Improved Production of Large Quantities of Highly Spin-Polarized Xenon for Use in Magnetic Resonance Applications*.” Gower Summer Research Symposium. Southern Illinois University, Carbondale, IL, 09/10/2009 (*Invited Talk*).

Conference Proceedings:

- (49). P. Constantinou, J. Liu, J. Hu, J. Davis, N. Z. Millward, **N. Whiting**, D. Menter, P. Bhattacharya, D. Carson. *Molecular Imaging of Mucin-Expressing Colon Tumors using Targeted Hyperpolarized Silicon Nanoparticles*. Cancer Prevention Research Institute of Texas (CPRIT) Annual Conference, Austin, TX, 11/9-10, 2015 (*abstract submitted*).
- (48). \***N. Whiting**, J. Hu, P. Bhattacharya. *Benefits, Limitations, and Improving the Future of MRI-Guided Endovascular Catheter Tracking*. 23<sup>rd</sup> International Society of Magnetic Resonance in Medicine, Toronto, Canada, 05/30-06/05, 2015. \*Abstract selected for Magna cum laude prize status.
- (47). \***N. Whiting**, J. Hu, N. Millward, R. Rupaimoole, D. Gorenstein, A. Sood, P. Bhattacharya. *Developing Hyperpolarized Silicon Micro and Nanoparticles for Targeted Molecular Imaging of Ovarian Cancer*. 23<sup>rd</sup> International Society of Magnetic Resonance in Medicine, Toronto, Canada, 05/30-06/05, 2015.\*Selected for 1<sup>st</sup> place E-poster presentation in the Molecular & Cellular Imaging Study Group Session.
- (46). J. Hu, **N. Whiting**, P. Constantinou, N.Z. Millward, D. Menter, D. Carson, P. Bhattacharya. *Towards Targeted Molecular Imaging of Colorectal Cancer by Hyperpolarized Silicon Particles Functionalized with Mucin Antibody*. 23<sup>rd</sup> International Society of Magnetic Resonance in Medicine, Toronto, Canada, 05/30-06/05, 2015 (*Talk*).
- (45). **N. Whiting**, J. Hu, J. Shaw, M. Cassidy, E. Cressman, C. Marcus, P. Bhattacharya. *Real-Time MRI-Guided Passive Catheter Tracking Using Hyperpolarized Silicon Nanoparticles*. Gordon Research Conference for *In Vivo* Magnetic Resonance, Andover NH, 07/27-08/01, 2014.
- (44). J. Hu, **N. Whiting**, J. Shah, N. Millward, M. Cassidy, E. Cressman, C. Marcus, D. Gorenstein, A. Sood, P. Bhattacharya. *Hyperpolarized <sup>29</sup>Si Magnetic Resonance—Towards Applications in MR Guided Catheter Tracking and Targeted Imaging of Cancer*. International Council on Magnetic Resonance in Biological Systems (ICMRBS), Dallas TX, 08/24-29, 2014 (*Talk*).
- (43). **N. Whiting**, J. Hu, M. Cassidy, P.E. Constantinou, N.Z. Millward, D.E. Volk, D.G. Gorenstein, D.D. Carson, C. Marcus, P. Bhattacharya. *Targeted MRI In Vivo by Hyperpolarized Silicon Nanoparticles*. 22<sup>nd</sup> International Society of Magnetic Resonance in Medicine, Milan, Italy, 05/10-16, 2014.
- (42). H. Newton, J. Skinner, J. Birchall, **N. Whiting**, B.M. Gust, K. Ranta, M.J. Barlow, B.M. Goodson. *Can We Utilise Rb/Cs Hybrid Optical Pumping to Hyperpolarise Noble Gases?* 55<sup>th</sup> Experimental Nuclear Magnetic Resonance Conference, Boston MA, 03/23-28, 2014 (*Talk*).
- (41). J. Skinner, H. Newton, J. Birchall, **N. Whiting**, M.J. Barlow, B.M. Goodson. *Using in situ Raman and NMR Spectroscopies to Map the Dependencies of Spin-Exchange Optical Pumping and Energy Transport on Xenon Density*. 55<sup>th</sup> Experimental Nuclear Magnetic Resonance Conference, Boston MA, 03/23-28, 2014.
- (40). M. Cassidy, **N. Whiting**, J. Hu, H. Chan, D. Gorenstein, D. Carson, C. Marcus, P. Bhattacharya. *“Background-Free Imaging Applications of Hyperpolarized Silicon Particles with <sup>29</sup>Si MRI”*. 4<sup>th</sup> International Symposium in DNP. Copenhagen, Denmark, 08/28-31, 2013. (*Talk*)
- (39). J. Shaw, **N. Whiting**, J. Hu, P. Bhattacharya. *“Catheter Tracking In Vivo by Magnetic Resonance Imaging Employing Hyperpolarized Silicon Nanoparticles”*. World Molecular Imaging Conference, Savannah, GA, 09/16-20, 2013.
- (38). **N. Whiting**, J. Hu, N. Zacharias, M. Ramirez, J. Bankson, L. Rao, D. Volk, D. Gorenstein, A. Sood, D. Menter, M. Frazier, P. Bhattacharya. *“Towards the Implementation of Hyperpolarized, Functionalized Silicon Nanoparticles as In Vivo Molecular Imaging Agents for the Early Detection of Cancer by Magnetic Resonance Imaging”*. MD Anderson Postdoctoral Science Symposium, The University of Texas MD Anderson Cancer Center, Houston, TX, 08/01/2013.
- (37). **N. Whiting**, J. Hu, M. Cassidy, N. Millward, D. Menter, M. Frazier, C. Marcus, P. Bhattacharya. *“Towards the Implementation of Hyperpolarized, Functionalized Silicon Nanoparticles as In Vivo Colorectal Molecular Imaging Agents”*. 21<sup>st</sup> International Society of Magnetic Resonance in Medicine. Salt Lake City, 04/20-26, 2013.


- (36). N. Millward, M. Cassidy, M. Lingwood, N. Sailasuta, **N. Whiting**, J. Hu, S. Han, B. Ross, C. Marcus, P. **Bhattacharya**. "Towards Real-time Metabolic and Molecular Imaging of Cancer by Three Different Modalities of Hyperpolarization". 21<sup>st</sup> International Society of Magnetic Resonance in Medicine. Salt Lake City, 04/20-26, 2013.
- (35). M. Cassidy, H. Chan, J. Hu, **N. Whiting**, C. Marcus, P. Bhattacharya. "Nuclear Spin Properties of Hyperpolarized Solid-State MRI Agents". 21<sup>st</sup> International Society of Magnetic Resonance in Medicine. Salt Lake City, 04/20-26, 2013.
- (34). J. Hu, N. Millward, M. Cassidy, M. Lingwood, N. Sailasuta, **N. Whiting**, S. Han, B. Ross, C. Marcus, P. Bhattacharya. "Towards In Vivo Real-time Metabolic and Targeted Molecular Imaging of Cancer via Hyperpolarized Magnetic Resonance". 54<sup>th</sup> Experimental Nuclear Magnetic Resonance Conference. Pacific Grove, CA, 04/14-19, 2013 (Talk).
- (33). H. Newton, J. Smith, L. Walkup, **N. Whiting**, M. Barlow, P. Morris, B. Goodson. "Effects of Gas Composition on Optical Pumping and Energy Transport for Hyperpolarized  $^{129}\text{Xe}$  Using in situ Raman Spectroscopy and NMR". 54<sup>th</sup> Experimental Nuclear Magnetic Resonance Conference. Pacific Grove, CA, 04/14-19, 2013.
- (32). **N. Whiting**, J. Hu, N. Zacharias, D. Volk, D. Gorenstein, A. Sood, P. Bhattacharya. "Hyperpolarized Silicon Nanoparticles Functionalized with Thioaptamers—Towards In Vivo MRI Targeting of Ovarian Cancer". 54<sup>th</sup> Experimental Nuclear Magnetic Resonance Conference. Pacific Grove, CA, 04/14-19, 2013.
- (31). K. Ranta, L. Walkup, **N. Whiting**, B. Gust, H. Newton, J. Smith, M. Barlow, B. Goodson. "SEOP Diagnostics: Exploring Alkali Metal ESR Polarimetry Under Conditions with Poorly Resolved Resonances". 54<sup>th</sup> Experimental Nuclear Magnetic Resonance Conference. Pacific Grove, CA, 04/14-19, 2013.
- (30). P. Nikolaou, A. Coffey, L. Walkup, B. Gust, **N. Whiting**, H. Newton, I. Muradyan, M. Dabaghyan, K. Ranta, G. Moroz, M. Rosen, S. Patz, M.J. Barlow, E. Chekmenev, S. Xu, A. Yilmaz, P. He, M. Gemeinhardt, Y. Gao, & B.M. Goodson. "High (~30-90%)  $^{129}\text{Xe}$  Hyperpolarization at High Xe Densities Using an 'Open-Source' Polarizer for Clinical and Materials MRS/MRI". 54<sup>th</sup> Experimental Nuclear Magnetic Resonance Conference. Pacific Grove, CA, 04/14-19, 2013.
- (29). **N. Whiting**, J. Hu, M. Cassidy, M. Ramirez, J. Bankson, N. Zacharias, D. Menter, M. Frazier, S. Kopetz, C. Marcus, P. Bhattacharya. "Towards the Implementation of Functionalized Silicon Nanoparticles as Long-Lived Hyperpolarized MRI Contrast Agents to be Used for the Early Detection of Colorectal Cancer". Global Academic Programs Conference (GAP), The University of Texas MD Anderson Cancer Center, Houston, TX, April 3-5, 2013.
- (28). H. Newton, **N. Whiting**, M.J. Barlow, P. Morris, L. Walkup, and B.M. Goodson. "In Situ Raman Spectroscopy to Determine  $\text{N}_2$  Gas Temperatures in Spin-Exchange Optical Pumping Cells for Use in Hyperpolarised Noble Gas NMR/MRI. EUROMAR & Xemat; Dublin, Ireland, June 27-July 5, 2012.
- (27). H. Newton, **N. Whiting**, M.J. Barlow, P. Morris, L. Walkup, and B.M. Goodson. "Effects of various spin-exchange optical pumping conditions on gas temperatures measured by Raman spectroscopy during production of hyperpolarised  $^{129}\text{Xe}$ . (Talk) XeMat; Dublin, Ireland, June 27-29, 2012.
- (26). P. Nikolaou, A. Coffey, L. Walkup, B. Gust, **N. Whiting**, H. Newton, I. Muradyan, M. Dabaghyan, K. Ranta, G. Moroz, M. Rosen, S. Patz, M.J. Barlow, E. Chekmenev, & B.M. Goodson. "'Scaling up' Fundamental Studies of SEOP at High Xe densities and Laser Fluxes to Create an 'Open-Source' Xe Polarizer for Clinical-Scale NMR and MRI". XeMat; Dublin, Ireland, June 27-29, 2012.
- (25). P. Nikolaou, A. Coffey, L. Walkup, B. Gust, **N. Whiting**, H. Newton, I. Muradyan, M. Dabaghyan, K. Ranta, G. Moroz, M. Rosen, S. Patz, M.J. Barlow, E. Chekmenev, S. Xu, A. Yilmaz, P. He, M. Gemeinhardt, Y. Gao, & B.M. Goodson. "New Developments for using hyperpolarized  $^{129}\text{Xe}$  and SPIONS as contrast agents: 1) 'Scaling-up' high-[Xe] SEOP for an 'Open-Source' clinical scale Xe polarizer; 2) Towards physiologically pH-sensing with dendron-functionalized SPIONs." EUROMAR; Dublin, Ireland, July 1-5, 2012.

- (24). **N. Whiting**, H. Newton, M.J. Barlow, P. Morris, and B.M. Goodson. "In Situ Raman Mapping of Gas Temperatures in Spin-Exchange Optical Pumping Cells for Use in Hyperpolarized Noble Gas NMR/MRI." 53<sup>th</sup> Experimental Nuclear Magnetic Resonance Conference (ENC): Miami, FL; April 15- 20, 2012.
- (23). P. Nikolaou, A. Coffey, L. Walkup, B. Gust, **N. Whiting**, H. Newton, S. Barcus, I. Muradyan, G. Moroz, M. Rosen, S. Patz, M.J. Barlow, E. Chekmenev, & B.M. Goodson. "An 'Open-Source' <sup>129</sup>Xe Polarizer for Clinical Imaging, in vivo MRS/MRI, and NMR/MRI of Porous Materials." 53<sup>th</sup> Experimental Nuclear Magnetic Resonance Conference (ENC): Miami, FL; April 15- 20, 2012.
- (22). **N. Whiting**, M.J. Barlow, H. Newton, L. Walkup, P. Nikolaou, & B.M. Goodson. "Improved Production of Hyperpolarized Xenon Using Cesium/Xenon Spin-Exchange Optical Pumping with High-Power, Frequency-Narrowed Laser Diode Arrays and High Xenon Partial Pressures." Frontiers of Biomedical Imaging Science Conference: Nashville, TN; June 13-16, 2011.
- (21). P. Nikolaou, A. Coffey, L. Walkup, B. Gust, **N. Whiting**, G. D. Moroz, E. Chekmenev, M.J. Barlow, S. Patz, M. Rosen, & B.M. Goodson. "Towards the Development of an 'Open-Source' High Volume <sup>129</sup>Xe/SEOP Apparatus for Potential Application in Human Lung Imaging and NMR/MRI Studies of Porous Materials". Frontiers of Biomedical Imaging Science Conference, Nashville, TN; June 13-16, 2011.
- (20). **N. Whiting**, M.J. Barlow, H. Newton, L. Walkup, P. Nikolaou, & B.M. Goodson. "Cesium/Xenon Spin-Exchange Optical Pumping Using High-Power, Frequency-Narrowed Laser Diode Arrays at High Xenon Densities." 52<sup>th</sup> Experimental Nuclear Magnetic Resonance Conference (ENC): Pacific Grove, CA; April 10- 15, 2011.
- (19). M. Liljeroth, **N. Whiting**, H. Newton, M.J. Barlow, R.J. Walker, K. Teh, B.M. Goodson, & P. Morris. "Continuous Flow Rb/<sup>129</sup>Xe Spin-Exchange Optical Pumping at High Xenon Densities: Preliminary Studies Towards in vivo Lung Imaging." 52<sup>th</sup> Experimental Nuclear Magnetic Resonance Conference (ENC): Pacific Grove, CA; April 10- 15, 2011.
- (18). K. Ranta, L. Walkup, **N. Whiting**, P. Nikolaou, M.J. Barlow, & B.M. Goodson. "Interplay of Temperature, Xe Density, and Laser Linewidth During Rb/<sup>129</sup>Xe Spin-Exchange Optical Pumping: Simulation vs. Experiment." 52<sup>th</sup> Experimental Nuclear Magnetic Resonance Conference (ENC): Pacific Grove, CA; April 10- 15, 2011.
- (17). **N. Whiting**, M.J. Barlow, P. Nikolaou, N. Eschmann, & B.M. Goodson. "Direct Comparison of Cs D<sub>1</sub>, D<sub>2</sub>, and Rb D<sub>1</sub> Spin-Exchange Optical Pumping for Generating Hyperpolarized Xenon for Large-Scale NMR/MRI Applications." 16<sup>th</sup> British Chapter of the International Society of Magnetic Resonance in Medicine (BC-ISMRM): Nottingham, UK; September 1-3, 2010.
- (16). **N. Whiting**, P. Nikolaou, N. Eschmann, M.J. Barlow, B.M. Goodson. "Cesium/Xenon Spin-Exchange Optical Pumping using High-Power Laser Diode Arrays at the Cs D<sub>1</sub> & D<sub>2</sub> Wavelengths." 51<sup>th</sup> Experimental Nuclear Magnetic Resonance Conference (ENC): Daytona Beach, FL April 18-23, 2010.
- (15). M. J. Barlow, N. Eschmann, **N. Whiting**, P. Nikolaou, B. M. Goodson. "Using High-Power Tunable 'On-Chip' Grating-Narrowed Laser Diode Arrays to Study the Interplay of Wavelength, Offset, Temperature, and Xe Density During Xe SEOP." 51<sup>th</sup> Experimental Nuclear Magnetic Resonance Conference (ENC): Daytona Beach, FL; April 18-23, 2010.
- (14). P. He, L. Walkup, **N. Whiting**, P. Nikolaou, K. E. Chaffee, X. Li, B. M. Goodson. "Studies of <sup>129</sup>Xe to <sup>1</sup>H Spin Polarization Transfer in Aqueous Xenon-Binding Systems." 51<sup>th</sup> Experimental Nuclear Magnetic Resonance Conference (ENC): Daytona Beach, FL; April 18-23, 2010.
- (13). M. J. Barlow, N. Eschmann, **N. Whiting**, P. Nikolaou, B. M. Goodson. "New Developments in <sup>129</sup>Xe SEOP with VHG-Narrowed Lasers for NMR/MRI Applications." 38<sup>th</sup> Southeastern Magnetic Resonance Conference (SEMRC). Vanderbilt University, Nashville, TN; Nov. 6-8, 2009.
- (12). B.M. Goodson, **N. Whiting**, P. Nikolaou, N. Eschmann, M.J. Barlow. "Preparation of Laser-Polarized Xenon at High Xe Densities and High Resonant Laser Powers Provided by Volume Holographic Grating-Narrowed LDAs." (Talk) 40<sup>th</sup> Division of Atomic, Molecular, & Optical Physics (DAMOP) of the American Physical Society: University of Virginia, Charlottesville, VA; May 19-23, 2009.

- (11). **N. Whiting**, P. Nikolaou, N. Eschmann, M.J. Barlow, B.M. Goodson. *“Interplay of Cell Temperature and Xenon Density Resulting in Anomalous High Xe Polarization during Optical Pumping at High Xe Densities.”* 50<sup>th</sup> Experimental Nuclear Magnetic Resonance Conference (ENC): Pacific Grove, CA; March 29- April 3, 2009.
- (10). M.J. Barlow, **N. Eschmann**, **N. Whiting**, P. Nikolaou, B.M. Goodson. *“Investigation of Xenon Nuclear Polarization as a Function of Laser Wavelength and Optical Power Using Narrowed Laser Sources.”* 50th Experimental Nuclear Magnetic Resonance Conference (ENC): Pacific Grove, CA; March 29- April 3, 2009.
- (9). **M. J. Barlow**, **N. Whiting**, P. Nikolaou, N. Eschmann, R. Mair, B. M. Goodson. *“A New Spin Exchange Optical Pumping (SEOP) Modality for Hyperpolarized <sup>129</sup>Xe Production and Use in Porous Media.”* 9<sup>th</sup> Magnetic Resonance in Porous Media Conference (MRPM9). Cambridge, MA; July 13-17, 2008.
- (8). **M. J. Barlow**, P. Nikolaou, **N. Whiting**, N. Eschmann, B. M. Goodson. *“Anomalous High Xenon Polarization at High Xenon Partial Pressures with Tunable Volume Holographic Grating (VHG) Frequency Narrowed Lasers.”* EUROMAR. St. Petersburg, Russia; July 6-11, 2008.
- (7). **N. Whiting**, P. Nikolaou, N. Eschmann, M.J. Barlow, B.M. Goodson. *“Effects of Power, Linewidth, and Component Gas Densities on Xenon Polarization with Fixed-Frequency Volume Holographic Grating (VHG)-Narrowed Laser Diode Arrays.”* 49<sup>th</sup> Experimental Nuclear Magnetic Resonance Conference (ENC): Pacific Grove, CA; March 9-14, 2008.
- (6). **M. J. Barlow**, P. Nikolaou, **N. Whiting**, N. Eschmann, B.M. Goodson, C.H. Li, R.W. Mair, M.S. Rosen, R.L. Walsworth. *“A Next-Generation Xenon-Polarization Laser source with Adjustable Wavelength, Spectral Width, and Flux for Biomedical and Materials Spectroscopy and Imaging.”* 49<sup>th</sup> Experimental Nuclear Magnetic Resonance Conference (ENC): Pacific Grove, CA; March 9-14, 2008.
- (5). P. Nikolaou, **N. Whiting**, K.E. Chaffee, I. Saha, M.J. Barlow, B.M. Goodson. *“Improved generation of laser-polarized xenon using a fiber-coupled laser diode array narrowed with an integrated volume holographic grating.”* 48<sup>th</sup> Experimental Nuclear Magnetic Resonance Conference (ENC): Daytona Beach, FL; April 22-27, 2007.
- (4). **M.J. Barlow**, C.H. Li, R.W. Mair, M.S. Rosen, R.L. Walsworth, **N. Whiting**, P. Nikolaou, K. Chaffee, I. Saha, B.M. Goodson. *“Volume holographic grating frequency narrowed laser for improved <sup>3</sup>He and <sup>129</sup>Xe Polarization for use with in materials, porous media, and lung MRI studies.”* 48<sup>th</sup> Experimental Nuclear Magnetic Resonance Conference (ENC): Daytona Beach, FL April 22-27, 2007.
- (3). **X. Li**, B. Musick, **N. Whiting**, B. M. Goodson. *“Site-specific interactions between xenon and a diamagnetic, structurally intact myoglobin in solution”* 47<sup>th</sup> Experimental Nuclear Magnetic Resonance Conference (ENC): Pacific Grove, CA; April 23-28, 2006.
- (2). **I. Saha**, P. Nikolaou, **N. Whiting**, X. Li, B.M. Goodson. *“An inexpensive, modular optical pumping apparatus for use in laser-polarized <sup>129</sup>Xe NMR experiments.”* 46<sup>th</sup> Experimental Nuclear Magnetic Resonance Conference (ENC): Providence, RI; April 10-15, 2005.
- (1). **B.M. Goodson**, X. Li, K. Chaffee, I. Saha, C. Newberry, P. Nikolaou, **N. Whiting**, M. Marjanska. *“Enhancing the NMR signatures of weak intermolecular interactions using laser-polarized xenon and liquid crystalline matrices.”* (Invited Talk). 229<sup>th</sup> American Chemical Society (ACS) National Meeting: San Diego, CA; March 13-17, 2005.

*Last updated: 14 August 2015*

# SCIENTIFIC REPORTS



OPEN

## Real-Time MRI-Guided Catheter Tracking Using Hyperpolarized Silicon Particles

Nicholas Whiting<sup>1,\*</sup>, Jingzhe Hu<sup>1,2,\*</sup>, Jay V. Shah<sup>1,3</sup>, Maja C. Cassidy<sup>4</sup>, Erik Cressman<sup>5</sup>, Niki Zacharias Millward<sup>1</sup>, David G. Menter<sup>6</sup>, Charles M. Marcus<sup>7</sup> & Pratip K. Bhattacharya<sup>1</sup>

Received: 11 March 2015

Accepted: 13 July 2015

Published: 04 August 2015

Visualizing the movement of angiocatheters during endovascular interventions is typically accomplished using x-ray fluoroscopy. There are many potential advantages to developing magnetic resonance imaging-based approaches that will allow three-dimensional imaging of the tissue/vasculature interface while monitoring other physiologically-relevant criteria, without exposing the patient or clinician team to ionizing radiation. Here we introduce a proof-of-concept development of a magnetic resonance imaging-guided catheter tracking method that utilizes hyperpolarized silicon particles. The increased signal of the silicon particles is generated via low-temperature, solid-state dynamic nuclear polarization, and the particles retain their enhanced signal for  $\geq 40$  minutes—allowing imaging experiments over extended time durations. The particles are affixed to the tip of standard medical-grade catheters and are used to track passage under set distal and temporal points in phantoms and live mouse models. With continued development, this method has the potential to supplement x-ray fluoroscopy and other MRI-guided catheter tracking methods as a zero-background, positive contrast agent that does not require ionizing radiation.

In the United States, heart disease has been the leading cause of death for nearly a century<sup>1</sup>, with recent annual death tolls of approximately 600,000 people<sup>2</sup> and direct and indirect costs exceeding \$100 billion<sup>3</sup> per annum. Cardiovascular diagnostic and interventional methodologies require the use of endovascular catheterization for procedures such as angiography, angioplasty, ablation, stent placement, and valve repair. Furthermore, catheters are also frequently used in risk stratification of chemotherapy-induced cardiotoxicity<sup>4</sup> and embolization therapy of cancer patients<sup>5</sup>. Critical tracking of these catheters is typically accomplished by monitoring a radiopaque filler material embedded into the polymer walls of catheters using x-ray fluoroscopy<sup>6</sup>; this cardiovascular guidance approach allows for real-time feedback, high spatiotemporal resolution, and the ability to distinguish the position of the catheter relative to anatomical structures. However, x-ray fluoroscopy-guided catheter tracking suffers from limitations in soft tissue contrast, as well as difficulty in three-dimensional navigation<sup>6</sup>. To some extent, this is addressed using cone-beam CT image reconstruction, but with the added costs of increased radiation exposure and decreased soft tissue contrast. In the clinic, this technique typically requires refresh rates of 1–10 frames per second (FPS); these refresh rates, combined with procedure-related activities, can expose both the patient (direct exposure in the short term) and attending physician and team (scatter exposure over the long term) to ionizing radiation in a relatively short period of time (minutes to tens of minutes). This

<sup>1</sup>Department of Cancer Systems Imaging, The University of Texas MD Anderson Cancer Center, Houston, TX 77030.

<sup>2</sup>Department of Bioengineering, Rice University, Houston, TX 77030. <sup>3</sup>Department of Biomedical Engineering, The University of Texas at Austin, Austin, TX 78712. <sup>4</sup>Kavli Institute of NanoScience, Delft University of Technology, Delft, Netherlands. <sup>5</sup>Department of Interventional Radiology, The University of Texas MD Anderson Cancer Center, Houston TX 77030. <sup>6</sup>Department of Gastrointestinal Medical Oncology, The University of Texas MD Anderson Cancer Center, Houston TX, 77030. <sup>7</sup>Niels Bohr Institute, University of Copenhagen, Denmark. \*These authors contributed equally to this work. Correspondence and requests for materials should be addressed to P.K.B. (email: pkbhattacharya@mdanderson.org)

can be especially problematic for pediatric patients<sup>7</sup>, who not only have a much longer anticipated lifetime but also a greater potential for multiple procedures. Additional health concerns in patients that are attributed to the iodinated contrast media include nephropathy<sup>8</sup> and, less commonly, allergic reactions.

Magnetic resonance imaging (MRI)-guided catheter tracking is attractive due to its many potential benefits, including three-dimensional imaging of the interactions between soft tissues and the vasculature without using ionizing radiation. The use of MRI-based catheter guidance also allows clinicians to simultaneously monitor other physiologically-relevant criteria, including metabolism, temperature, blood flow velocity, and tissue perfusion<sup>9</sup>. To date, typical MRI-guided catheter guidance approaches fall into one of two categories: active or passive tracking. The former method involves monitoring the active signal of a miniature radiofrequency (rf) coil placed near the catheter tip<sup>10</sup>, while the latter may examine susceptibility differences between paramagnetic dysprosium oxide rings embedded into the catheter versus that of nearby tissue<sup>11</sup>. Other passive MR catheter tracking techniques include  $T_1$ -weighted imaging of a catheter filled with gadolinium<sup>12</sup>, or non  $^1\text{H}$ -imaging of catheters filled with other contrast media (including  $^{19}\text{F}$  imaging of perfluorooctylbromide<sup>13</sup> and  $^{13}\text{C}$  imaging of hyperpolarized (HP)  $^{13}\text{C}$ -labelled 2-hydroxyethylpropionate<sup>14</sup>). While these methods offer contrast between the otherwise MR-invisible catheter and patient anatomy, they also suffer from inherent drawbacks that limit their applicability in the clinic. For example, active catheter tracking methods require specialized catheters and dedicated rf circuitry/equipment, while posing the risk of localized tissue heating and steering problems due to the inflexibility of the catheter tip<sup>10</sup>. While passive susceptibility tracking is a relatively simple process by comparison to active imaging, it usually provides negative contrast that is vulnerable to distortion artefacts<sup>11</sup> and also requires the use of a specialized catheter.  $T_1$ -weighted imaging of gadolinium-filled catheters requires competition with a significant  $^1\text{H}$  noise background and  $T_2^*$ -associated signal losses<sup>12</sup>. In the case of hyperpolarized  $^{13}\text{C}$  tracer alternatives, a continuous supply of the contrast agent is required because these tracers naturally depolarize within a timeframe of 60 seconds, an effect that is hastened by magnetization-depleting rf pulses during signal acquisition<sup>14</sup> (a consequence that is true for all hyperpolarized media). Also, catheters that are filled with liquid MRI contrast agents (such as gadolinium or  $^{19}\text{F}$  and  $^{13}\text{C}$  tracers) cannot easily be used for simultaneously injecting other liquids into the body<sup>13</sup> without employing multi-lumen catheters, thereby limiting their clinical use for further diagnostic and/or interventional procedures.

A method of hyperpolarizing silicon micro- and nanoparticles has been recently demonstrated<sup>15,16</sup> to increase  $^{29}\text{Si}$  MR signals by up to 3–5 orders of magnitude via enhanced nuclear spin alignment, while retaining this improved signal for tens of minutes. Hyperpolarization of the  $^{29}\text{Si}$  nuclear spins is generated by solid-state dynamic nuclear polarization (DNP), which uses low temperatures and high magnetic fields to spin-polarize an electron bath to near unity; this spin polarization is then transferred to nearby nuclear spins through microwave-mediated dipolar interactions<sup>17</sup>. DNP of solid (dry) silicon particles takes advantage of naturally-occurring electronic defects on the particle surfaces and obviates the need for additional radicals to generate the necessary free electrons<sup>18</sup>. The resulting increase in  $^{29}\text{Si}$  nuclear spin polarization is relatively long-lasting ( $T_1 \sim 40$  minutes)<sup>15</sup> compared to other hyperpolarized modalities (e.g., HP  $^{13}\text{C}$  tracers)<sup>19</sup>, and is not affected by the *in vivo* environment. Silicon micro- and nanoparticles are non-toxic, non-radioactive, and have been investigated for biomedical applications due to their favorable biocompatibility and biodegradability<sup>20</sup>.

Here, we use solid-state hyperpolarized silicon particles as a proof-of-concept for MRI-based catheter guidance in both phantoms and *in vivo*. We demonstrate catheter tracking both over long time durations (40 minutes) and in real time (refresh rate of 6.25 FPS), as well as two-dimensional and three-dimensional catheter guidance visualization. This method of passive catheter tracking provides background-free positive contrast using a standard medical-grade catheter and does not require the catheter to be filled with a liquid tracer. The biocompatible silicon particles are commercially available and would contribute minimally to the cost of the procedure (the work presented here required  $\sim 3\text{¢}$  of silicon particles), and are hyperpolarized using a well-characterized<sup>21</sup> modality that has recently been made available for clinical studies of  $^{13}\text{C}$ -labeled metabolic tracers<sup>22</sup>. With further development, this approach could have a situational clinical role as a non-ionizing, zero-background, positive contrast imaging agent for real-time catheter guidance using MRI.

## Results

**Catheter tracking over long time durations.** Silicon particles (average mean diameter  $\sim 2\ \mu\text{m}$ ) were packed into sample tubes and hyperpolarized in the solid state using a home-built DNP device. Following hyperpolarization, the particles were collected, quickly warmed to room temperature, and affixed to the tip of a medical grade catheter. For this study, two silicon samples were used:  $\sim 50$  mg of particles loaded onto a 24 Fr urinary catheter (8 mm outer diameter, or 'OD'), and  $\sim 6$  mg of particles loaded onto a 5 Fr angiocatheter (1.67 mm OD). Additional experimental criteria are available in the Materials and Methods section, as well as the Supplementary Material.

As an initial proof-of-concept, Fig. 1a shows positive contrast  $^{29}\text{Si}$  images (co-registered with  $^1\text{H}$  imaging) of the urinary catheter transiting  $\sim 4$  cm through a gelatin phantom over the course of 40 minutes; this short distance is necessitated by the use of a  $^{29}\text{Si}/^1\text{H}$  dual-tuned MRI coil that was designed for *in vivo* mouse studies (active region of coil only 52 mm in z-axis). The extended time scale over which the particles retain their increased magnetization is consistent with previous silicon micro- and nanoparticle

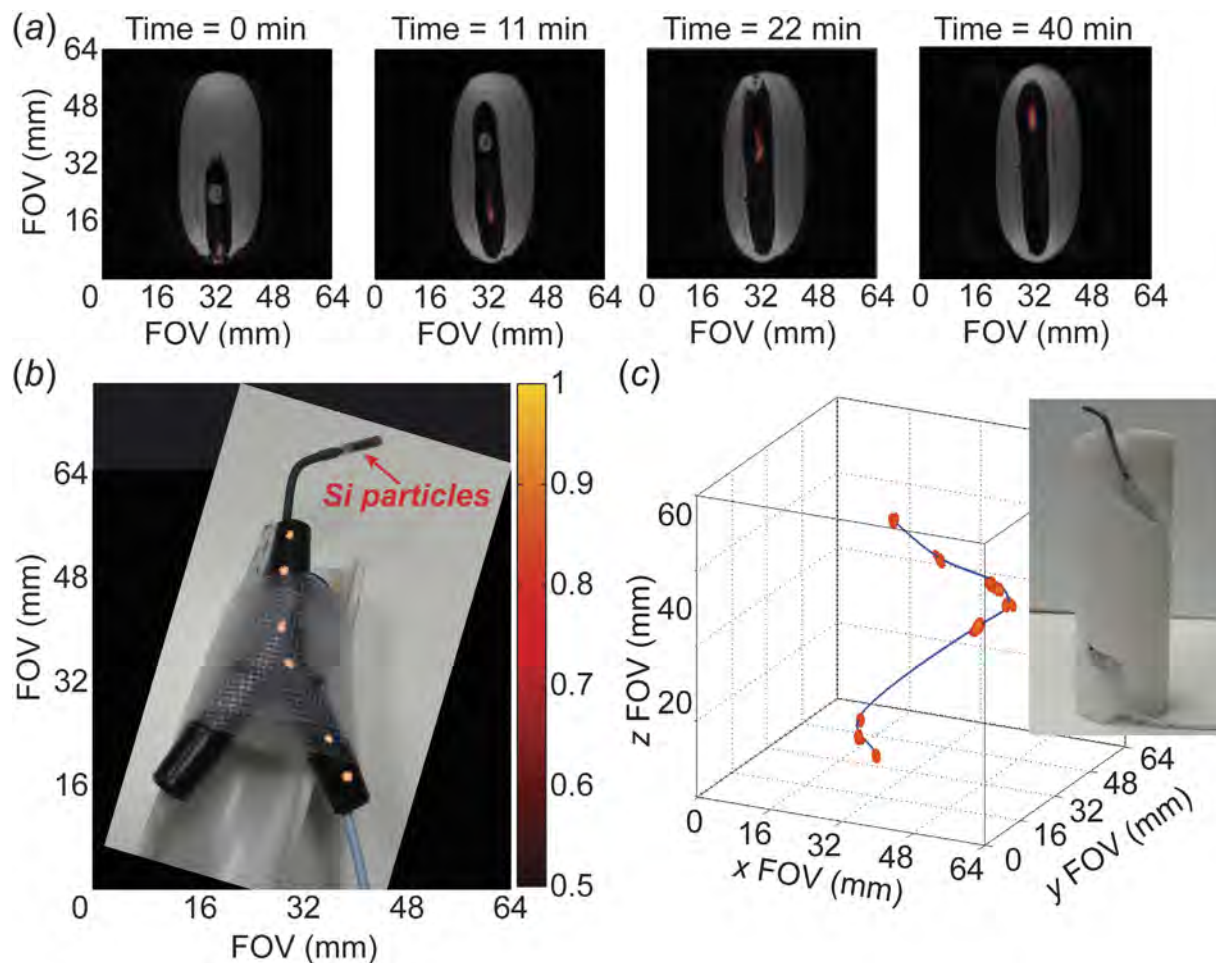


**Figure 1. HP  $^{29}\text{Si}$  particle MRI-tracking in phantoms.** (a) Transit of  $\sim 50$  mg of silicon particles loaded into a 24Fr urinary catheter moving  $\sim 4$  cm through a gelatin phantom over the course of 40 minutes; co-registered  $^{29}\text{Si}/^1\text{H}$  imaging shows the outline of the catheter in the void space left in the gelatin. (b) Angiocatheter (5Fr) loaded with  $\sim 6$  mg of silicon particles moving through Y-shaped hollow plastic phantom to simulate branching of vasculature; picture of catheter and phantom superimposed with a composite of  $^{29}\text{Si}$  MRI images. The sample tube containing silicon particles is push-fit onto the tip of the angiocatheter. (c) Angiocatheter tracking three-dimensional passage around a spiral phantom (*picture inset*). Absolute  $^{29}\text{Si}$  signal intensities (colored scale, arbitrary units) are consistent for (a)–(c); greyscale denotes  $^1\text{H}$  intensities. Pertinent imaging parameters, as well as Supplemental Video S1 (showing a rotating view of Fig. 1c), are included in the Supplementary Materials.

studies<sup>15,23</sup>, and is far greater than what is typically expected from other hyperpolarized species (e.g.,  $T_1$  of HP  $^{13}\text{C}$ -labelled tracers is typically  $\leq 1$  minute)<sup>24</sup>. The ability to acquire images over this time duration supports this method's future development for potential utility in the clinic.

**Multi-dimensional catheter tracking.** Following the initial catheter tracking demonstration using a large urinary catheter, we progressed to monitoring a medical-grade angiocatheter using roughly an order of magnitude fewer particles (corresponding to  $\sim 12\%$  of the previously available magnetization). This 5Fr catheter was tracked in two dimensions at distinct points over the course of  $\sim 4$  cm and 28 minutes as it transited through a plastic Y-shaped hollow phantom to simulate guidance through the branching of the vasculature (specifically, for typical retrograde common femoral artery access with the catheter tip positioned above the level of the simulated aortic bifurcation; Fig. 1b). Further visualization of angiocatheter maneuverability includes three-dimensional tracking through a spiral-shaped phantom (Fig. 1c; Supplemental Video S1).

***In vivo* catheter tracking.** Given that the 5Fr angiocatheter is similar in diameter to commercially available endoscopes used for mouse colonoscopies<sup>25</sup> as well as being a common size for human endovascular use, initial *in vivo* studies were carried out using the large intestine of a live mouse as a surrogate

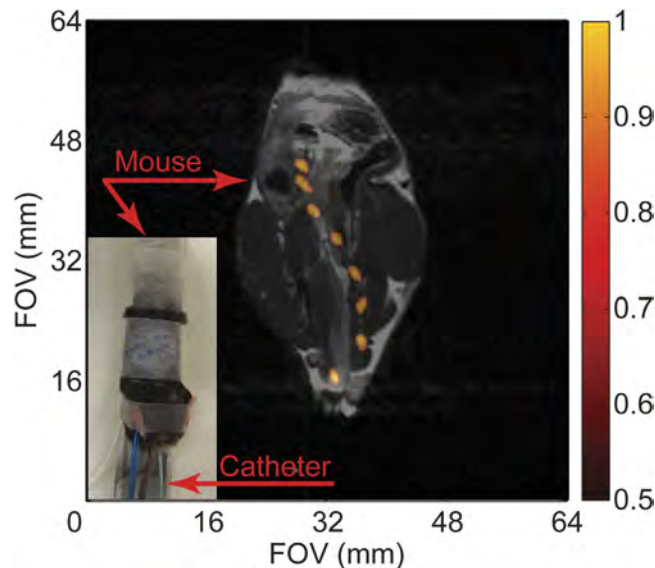


**Figure 2.** HP  $^{29}\text{Si}$  particle MRI-tracking *in vivo*. Composite of  $^{29}\text{Si}$  images (co-registered with single  $^1\text{H}$  anatomical scan) showing transit of angiocatheter loaded with silicon particles through the large intestines of a live normal mouse (*picture inset*) over the course of 4 min. Absolute  $^{29}\text{Si}$  signal intensities are denoted in arbitrary units on the colored scale; greyscale denotes  $^1\text{H}$  intensities. Pertinent imaging parameters, as well as Supplemental Video S2 (showing a time-lapse video of the catheter tracking in Fig. 2), are included in the Supplementary Materials.

for the human vasculature. The 5 Fr angiocatheter, loaded with silicon particles, was inserted into the rectum of a normal mouse and a series of  $^{29}\text{Si}$  imaging acquisitions was executed at discrete intervals while the catheter transited through the intestinal tract (Fig. 2; Supplemental Video S2; Supplemental Fig. S1). Following this series, a single  $^1\text{H}$  image was taken for anatomical co-registration; because the  $^1\text{H}$  image was acquired following the catheter movement, there is a slight discrepancy in the overlaid images due to a catheter-induced shifting of the large intestines, along with potential peristaltic responses by the gut that are not present in the single  $^1\text{H}$  scan. Subsequent studies utilized an alternating  $^{29}\text{Si}/^1\text{H}$  imaging protocol (Fig. 3; Supplemental Video S3) that shows the undulating of the intestines with the movement of the catheter. Regardless, the catheter is visualized moving in two dimensions  $\sim 3$  cm through the intestinal tract of the mouse over the course of  $\sim 4$  minutes ( $\sim 2$  cm in 22 min. for Fig. 3), demonstrating the first *in vivo* results using HP  $^{29}\text{Si}$  particles for catheter guidance.

**Real-time catheter tracking.** Because continuous imaging is requisite for catheter tracking in the clinic, we demonstrated this technique using real-time  $^{29}\text{Si}$  imaging of the urinary catheter transiting through a gelatin phantom (Fig. 4; Supplemental Video S4). The co-registered images show the catheter moving  $\sim 5$  cm over the course of 20 frames in  $\sim 3.2$  seconds (only 11 of the 20 frames shown here), resulting in a frame rate of 6.25 FPS. These image refresh rates are comparable to those that are typically achieved using fluoroscopy-guided catheter tracking in the clinic<sup>6</sup>. Longer time durations of continuous imaging are also possible using the same allotment of hyperpolarized particles (as the experiment was successfully repeated immediately afterwards with the same sample; *not shown*).

## Discussion

In this proof-of-concept study, we have demonstrated the viability of passive catheter tracking using hyperpolarized  $^{29}\text{Si}$  MRI using both phantoms and mouse models, over long time durations and in real time, and in both two and three dimensions. This method provides radiation-free, background-free positive contrast over the course of  $>40$  minutes using non-specialized catheters that are tagged with a biologically safe media. While current limitations in  $^{29}\text{Si}$  polarization level, MR hardware, and MR pulse sequences did not allow for real-time imaging (of several FPS) over the course of minutes, this advance will be critical to potential future clinical translation. With further development, co-registered  $^1\text{H}/^{29}\text{Si}$  MRI may find a role in clinical catheter tracking because of its ability to image the tissue/vasculature interface, as well as track other physiologically-relevant criteria. Compared to other MRI-guided catheter imaging techniques, it is not susceptible to rf burns, negative contrast, distortion artefacts, or competitive background signals.

The experiments presented here are limited by a reduced field of view that is inherent to small animal imaging coils that are designed for mouse imaging (35 mm inner diameter, or 'ID'; 52 mm homogenous rf region in z-axis); this is a result of the  $^{29}\text{Si}$  DNP polarizer being situated in a small animal imaging facility

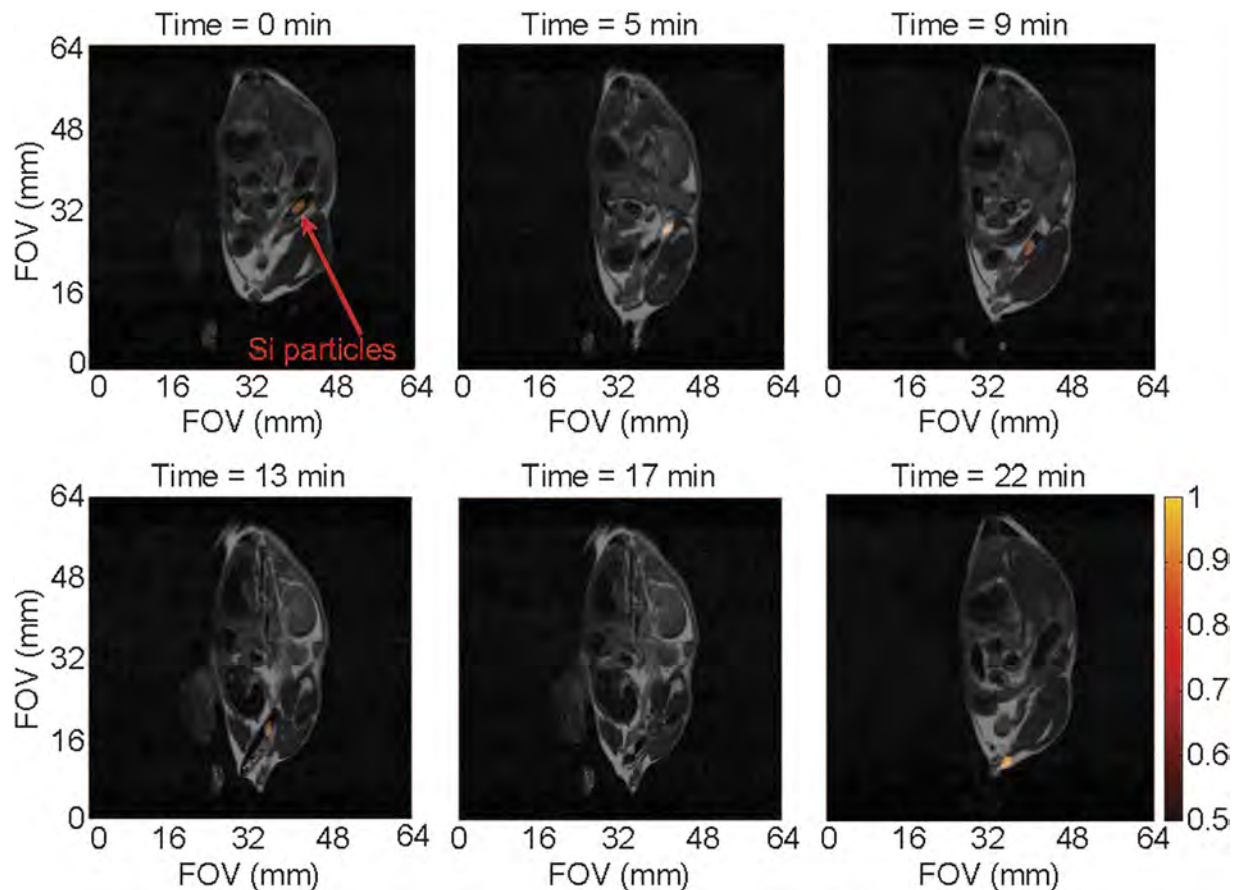


**Figure 3.** Co-registered  $^{29}\text{Si}/^1\text{H}$  MRI-tracking *in vivo*. Transit of angiocatheter through the large intestines of a live normal mouse using alternating  $^{29}\text{Si}/^1\text{H}$  scans, showing changes in mouse anatomy with movement of the catheter. Absolute  $^{29}\text{Si}$  signal intensities are denoted in arbitrary units on the colored scale; greyscale denotes  $^1\text{H}$  intensities. Pertinent imaging parameters, as well as Supplemental Video S3 (showing a time-lapse video of the catheter tracking in Fig. 3), are included in the Supplementary Materials.

without any clinical scanners in close proximity. Combined with this is a current lack of human-scale MRI detection coils that are tuned to the  $^{29}\text{Si}$  resonance frequency. Another potential drawback is the non-renewable nature of hyperpolarized signal; which decays through both natural spin population redistribution over time, as well as through the application of magnetization-depleting rf pulses for image acquisition. The  $^{29}\text{Si}$  signal in these particles can last for tens of minutes, which is on the same scale as most endovascular catheterization procedures. Also, the depletion of available magnetization upon the administration of rf pulses was mitigated by using small tipping angle pulses to minimally perturb the  $^{29}\text{Si}$  spins. For early acquisitions, a Fast Low-Angle Shot (FLASH) sequence employed a ramped tipping angle to provide near-constant  $^{29}\text{Si}$  signal intensities with each acquisition; the final image of the longer time duration experiments ended with a  $90^\circ$  Rapid Acquisition with Refocused Echos (RARE) sequence to maximize the amount of signal left at the end of the study. Given the short  $T_2^*$  of these silicon particles ( $\sim 600$  ms), additional gains could be achieved by employing a zero echo time (ZTE) imaging sequence to improve the signal-to-noise ratio with even smaller excitation pulses; it should also be noted that  $^{29}\text{Si}$  MRI scans were completed with single scans (no averaging required) and use high reconstruction thresholding due to zero  $^{29}\text{Si}$  signal background and *a priori* knowledge of the expected image profile. Furthermore, the long  $T_2$  (1–2 s) of these could be taken advantage of in order to image more lines of k-space with fewer rf pulses, and future improvements to the imaging hardware (i.e., flexible phased-array coils) can also be used to maximize scanning time by mitigating the deleterious effects of image acquisition. With moderate improvements to the  $^{29}\text{Si}$  hyperpolarization level, MR hardware, and pulse sequences, the spatial resolution in this study ( $\sim 1$  mm) may become more competitive with the current clinical standard of x-ray fluoroscopy ( $\sim 0.1$  mm).

Silicon-based micro- and nanoparticles have received recent interest as targeted diagnostic and drug delivery vehicles, due to their biocompatibility, biodegradability, and simple surface chemistry that is amenable to drug loading and targeting<sup>20</sup>. Because of this, they are favorable for development as platform nanotechnologies, where multiple targeting agents and therapeutic drugs can be attached to the particles surfaces for multiplexed theranostic applications. For this study, we chose larger silicon microparticles

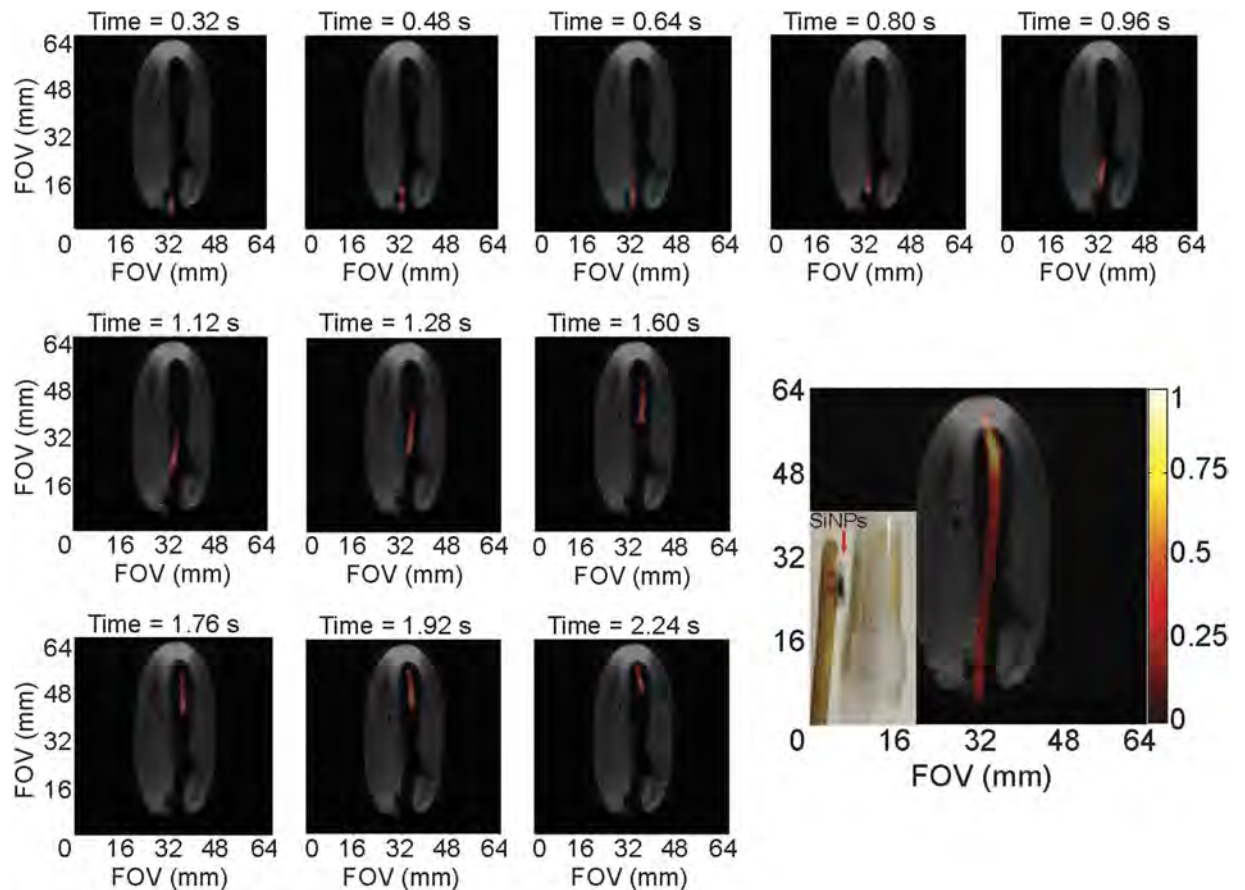


**Figure 4. Real-time  $^{29}\text{Si}$  MRI catheter tracking.** Individual scans showing movement of the large urinary catheter through a gelatin phantom at a frame rate of 6.25 FPS; bottom right figure shows composite of all twenty  $^{29}\text{Si}$  images (not all shown individually) over the course of 3.2 seconds. Co-registered with a single  $^1\text{H}$  scan (greyscale) after conclusion of  $^{29}\text{Si}$  images (colored scale). *Inset* picture shows silicon particles inside polarizing tube next to urinary catheter and gelatin phantom; during the experiment, the sample tube containing the silicon particles is placed inside the urinary catheter (utilizing the existing port near the catheter tip, *not shown*), where it rests between the two red horizontal lines drawn on the catheter. Pertinent imaging parameters, as well as Supplemental Video S4 (showing a real-time video of the catheter tracking in Fig. 4), are included in the Supplementary Materials.

because of their longer  $T_1$  compared to particles in the  $<100$  nm range ( $T_1 \sim 10\text{--}15$  min). The ability to hyperpolarize these particles makes them amenable to *in vivo* MR imaging<sup>15</sup>; since its gyromagnetic ratio is similar to those of  $^{13}\text{C}$  and  $^{15}\text{N}$ , the  $^{29}\text{Si}$  resonance frequency is typically within the tuning range of commercial (multinuclear) MRI systems. Increasing interest in clinical  $^{29}\text{Si}$  MRI may prompt the implementation of human-scale imaging coils that are resonant at the  $^{29}\text{Si}$  precession frequency; these coils may be able to improve on relative sensitivity (neglecting filling factor) using phased-array receiver configurations. Future studies will look to utilize clinical MRI scanners and torso  $^{29}\text{Si}$  imaging coils to expand the available field of view for catheter tracking.

The recent clinical demonstration of DNP of small  $^{13}\text{C}$ -metabolites<sup>22</sup> in prostate cancer patients, along with ongoing clinical trials of silicon-based particles for drug delivery<sup>26</sup>, should help pave the way for rapid translation of hyperpolarized  $^{29}\text{Si}$  MRI to the clinic. Although current versions of commercially-available clinical DNP devices are not marketed for silicon hyperpolarization, there should be no technical reason why it would not be feasible with minor alterations; in the future, using these devices for both  $^{13}\text{C}$  metabolic studies and  $^{29}\text{Si}$  molecular and interventional imaging could help defray hospital costs for access to hyperpolarized media. Furthermore, because the effects of hyperpolarization are field-independent, this technique is amenable for MRI at lower  $B_0$ , as well as in open-configuration scanners that are more conducive to interventional procedures. For this proof-of-concept work, the sample tube of hyperpolarized silicon particles was either push-fit onto the end of the angiocatheter, or placed inside the end of the urinary catheter; while we did not physically alter the catheter in any way, we recognize that improvements in silicon particle placement will be key to further development. To that end, future studies will attempt to coat the entirety of the catheter in hyperpolarized silicon particles to permit visualization of

the full catheter length (allowing bends and/or kinks to be monitored) while allowing the lumen to be used to inject contrast media, collect specimens, and conduct interventional operations and therapies. With further development, enhanced  $^{29}\text{Si}$  MRI-guided catheter visualization may allow clinicians to perform concurrent diagnostic and interventional MRI studies without the need to shuttle patients from one imaging suite to another, decreasing patient residence time and increasing safety.

## Materials and Methods

**$^{29}\text{Si}$  particles and catheters.** Silicon particles (polycrystalline/amorphous; average mean diameter  $\sim 2\ \mu\text{m}$ ) were commercially sourced (CAS No. 7440-21-3) and used as received (99.9985% elemental purity;  $^{29}\text{Si}$  isotopic natural abundance of  $\sim 4.7\%$ ). The particles were packed into small Teflon tubes; one sample (used for phantom experiments) contained  $\sim 50\ \text{mg}$  of particles packed into a 3 mm ID  $\times$  8 mm long tube and (following  $^{29}\text{Si}$  DNP) was placed inside the existing opening near the tip of the large urinary catheter (24 Fr; 8 mm OD; Rochester Medical Corp.), while the other sample (used for phantom and mouse experiments) consisted of  $\sim 6\ \text{mg}$  of particles packed into a 1.4 mm ID  $\times$  4.5 mm long tube and (following DNP) was push-fit onto the tip of the angiocatheter (5 Fr; 1.67 mm OD; Cook Medical). For hyperpolarization, the sample tubes were push-fit onto the end of a garolite rod and inserted into the DNP device (the smaller sample was placed inside of a larger sample tube, which was then push-fit onto the end of the garolite rod).

**$^{29}\text{Si}$  DNP.** After insertion of the packed sample tubes into the home-build polarizer, DNP was performed at  $\sim 3.2\ \text{K}$  and  $\sim 2.9\ \text{T}$ . Polarization times typically ranged from 5 hours for the larger (50 mg) sample to 17 hours for the smaller (6 mg) sample; the deciding factor for polarization time was the ability to generate sufficient  $^{29}\text{Si}$  signal to complete the imaging study (these silicon particles typically reached steady-state hyperpolarization after  $\sim 15\ \text{hrs}$  of DNP). The 100 mW microwave source was frequency-modulated from 80.83 to 80.90 GHz using a 20 kHz ramp modulation, and directed to the sample via waveguide and slot antenna. Quality control was monitored using an on-board miniature NMR spectrometer to sample  $^{29}\text{Si}$  polarization levels during DNP. The silicon particles can be quickly removed from the polarizer, warmed to room temperature, and affixed to the catheter tip without a significant loss in polarization; the low specific heat capacity (712 J/kg $^\circ\text{C}$ ) and robust thermal conductivity (159 W/m $^\circ\text{C}$ ) of silicon<sup>27</sup> allow the sample to be warmed by hand while transporting to the MRI scanner ( $T_{\text{transport}} < 1\ \text{minute}$ ). The measured hyperpolarized relaxation rate of the silicon particles was  $\sim 25\ \text{minutes}$  at 7 T and room temperature.

**MRI experiments.** All imaging experiments described here were performed in a 7 T horizontal-bore small animal scanner (Bruker Biospin), using Paravision software (v5.1; Bruker Biospin). A custom-made dual-tuned  $^1\text{H}/^{29}\text{Si}$  litz coil (Doty Scientific) was used for co-registered imaging (35 mm ID; homogenous rf region  $\sim 52\ \text{mm}$  along z-axis). A small sample of silicon oil (1.5 ml; CAS: 63148-62-9) was used for calibration purposes; typical  $^{29}\text{Si}$  nuclear spin polarization values ranged from 0.5–1.0%.  $^{29}\text{Si}$  imaging was performed using Fast Low Angle Shot (FLASH) and Rapid Acquisition with Refocused Echoes (RARE) sequences;  $^1\text{H}$  anatomical and phantom images used a RARE sequence in the coronal plane. Additional details of the imaging sequences and processing protocols are listed in the Supplementary Materials.

**Phantom experiments.** Phantoms were positioned in the center of the homogenous rf region of the MRI coil, and the HP  $^{29}\text{Si}$ -tagged catheter was moved through the phantom during imaging acquisitions. Phantoms consisted of gelatin inside a 50 ml centrifuge tube (Figs 1a and 4), a 3-way plastic hose barb connector (Fig. 1b), and a spiral groove etched into the side of a 32 mm diameter  $\times$  98 mm long cylindrical stock of PTFE (Fig. 1c).

**Mouse handling.** All animal studies were performed in accordance with animal use protocols that were approved by the UT MD Anderson Cancer Center “Institutional Animal Care and Use Committee” (IACUC). Wild type male APC<sup>(+/+)</sup> mice with a BL6 background (DOB 12/25/2013; sourced from MD Anderson Cancer Center) were used in all studies; these non-genetically modified mice (tail genotyping) were produced in an APC<sup>MIN</sup> breeding colony. These normal mice were anesthetized with 2% isoflurane (in 0.75 l/min oxygen) administered by an MR-compatible nose cone while the mouse was stationed on a custom cradle inside the MRI coil. The HP  $^{29}\text{Si}$ -tagged 5 Fr angiocatheter was inserted  $\sim 3\ \text{cm}$  into the rectum of the live mouse; it was then slowly pulled out in discrete intervals corresponding to the given imaging sequence. For Fig. 2; a single  $^1\text{H}$  image was acquired after the series of  $^{29}\text{Si}$  images. For Fig. 3, alternating  $^{29}\text{Si}$  and  $^1\text{H}$  images were acquired. All mice survived the procedure with no evidence of ill effects.

## References

- Greenlund, K. J. *et al.* in *Silent Victories: The History and Practice of Public Health in Twentieth Century America* (eds J. W. Ward & C. Warren) Ch. 18, 381 (Oxford University Press, 2006).
- Murphy, S. L., Xu, J. Q. & Kochanek, K. D. Deaths: Final data for 2010. *National Vital Statistics Reports* **61** (2013).
- Heidenreich, P. A. *et al.* Forecasting the future of cardiovascular disease in the United States: a policy statement from the American Heart Association. *Circulation* **123**, 933–944 (2011).

4. Bovelli, D., Platanoitis, G. & Roila, F. Cardiotoxicity of chemotherapeutic agents and radiotherapy-related heart disease: ESMO Clinical Practice Guidelines. *Annals of Oncology* **21**, 277–282 (2010).
5. Goode, J. A. & Matson, M. B. Embolisation of cancer: what is the evidence? *Cancer Imaging* **4**, 133–141 (2004).
6. Ma, Y. *et al.* Real-time x-ray fluoroscopy-based catheter detection and tracking for cardiac electrophysiology interventions. *Medical Physics* **40**, 071902 (2013).
7. American Academy of Pediatrics: Committee on Environmental Health. Risk of ionizing radiation exposure to children: a subject review. *Pediatrics* **101**, 717–719 (1998).
8. McCullough, P. A., Wolyn, R., Rocher, L. L., Levin, R. N. & O'Neill, W. W. Acute renal failure after coronary intervention: incidence, risk factors, and relationship to mortality. *The American Journal of Medicine* **103**, 368–375 (1997).
9. Bartles, L. W. & Bakker, C. J. G. Endovascular interventional magnetic resonance imaging. *Physics in Medicine and Biology* **48**, R37–R64 (2003).
10. Dumoulin, C. L., Souza, S. P. & Darrow, R. D. Real-time position monitoring of invasive devices using magnetic resonance. *Magnetic Resonance in Medicine* **29**, 411–415 (1993).
11. Bakker, C. J. *et al.* MR-guided endovascular interventions: susceptibility-based catheter and near-real-time imaging technique. *Radiology* **202**, 273–276 (1997).
12. Omary, R. A. *et al.* Real-time MR imaging-guided passive catheter tracking with use of gadolinium-filled catheters. *Journal of Vascular and Interventional Radiology* **11**, 1079–1085 (2000).
13. Kozerke, S. *et al.* Catheter tracking and visualization using  $^{19}\text{F}$  nuclear magnetic resonance. *Magnetic Resonance in Medicine* **52**, 693–697 (2004).
14. Magnusson, P. *et al.* Passive catheter tracking during interventional MRI using hyperpolarized  $^{13}\text{C}$ . *Magnetic Resonance in Medicine* **57**, 1140–1147 (2007).
15. Cassidy, M., Chan, H. R., Ross, B. D., Bhattacharya, P. K. & Marcus, C. M. *In vivo* magnetic resonance imaging of hyperpolarized silicon nanoparticles. *Nature Nanotechnology* **8**, 363–368 (2013).
16. Atkins, T. M. *et al.* Synthesis of long  $T_1$  silicon nanoparticles for hyperpolarized  $^{29}\text{Si}$  magnetic resonance imaging. *ACS Nano* **7**, 1609–1617 (2013).
17. Ardenkjaer-Larsen, J. H. *et al.* Increase in signal-to-noise ratio of  $>10,000$  times in liquid-state NMR. *Proceedings of the National Academy of Sciences of the USA* **100**, 10158–10163 (2003).
18. Cassidy, M., Ramanathan, C., Cory, D. G., Ager, J. W. & Marcus, C. M. Radical-free dynamic nuclear polarization using electronic defects in silicon. *Physical Review B* **87**, 161306(R) (2013).
19. Golman, K., Zandt, R., Lerche, M. H., Pehrson, J. & Ardenkjaer-Larsen, J. H. Metabolic imaging by hyperpolarized  $^{13}\text{C}$  magnetic resonance imaging for *in vivo* tumor diagnosis. *Cancer Research* **66**, 10855–10860 (2006).
20. Park, J.-H. *et al.* Biodegradable luminescent porous silicon nanoparticles for *in vivo* applications. *Nature Materials* **8**, 331–336 (2009).
21. Yen, Y.-F., Nagasawa, K. & Nakada, T. Promising application of dynamic nuclear polarization for *in vivo*  $^{13}\text{C}$  MR imaging. *Magnetic Resonance in Medicine* **10**, 211–217 (2011).
22. Nelson, S. J. *et al.* Metabolic imaging of patients with prostate cancer using hyperpolarized  $[1-^{13}\text{C}]$  pyruvate. *Science Translational Medicine* **5**, 198ra108 (2013).
23. Aptekar, J. W. *et al.* Silicon nanoparticles as hyperpolarized magnetic resonance imaging agents. *ACS Nano* **3**, 4003–4008 (2009).
24. Keshari, K. R. & Wilson, D. M. Chemistry and biochemistry of  $^{13}\text{C}$  hyperpolarized magnetic resonance using dynamic nuclear polarization. *Chemical Society Reviews* **43**, 1627–1659 (2014).
25. Becker, C., Fantini, M. & Neurath, M. High resolution colonoscopy in live mice. *Nature Protocols* **1**, 2900–2904 (2007).
26. Lehto, V.-P. & Riikonen, J. in *Porous Silicon for Biomedical Applications*. (ed. Santos, H.) Ch. 14, 335–350 (Woodhead Publishing, 2014).
27. Popescu, R. ISP Optics Datasheet; pg. 21. <http://www.ispoptics.com> (2015) (Date of Access: 02/05/2015).

## Acknowledgments

The authors would like to thank Drs. J. Kim and S. Kopetz (MDACC) for helpful discussions and Ms. L. Bitner (MDACC) for assistance with the animal studies. Funding: this work was funded by the MD Anderson Cancer Center Odyssey Postdoctoral Fellowship (NW), NCI R25T CA057730 (NW), CA016672 (NW), DoD PC131680 (NW), CPRIT Summer Undergraduate Research fellowship (JS), MDACC Institutional Research Grants (PB), MDACC Institutional Startup (PB, NW, JH), U54 CA151668 (PB), Leukemia and Brain SPORE Developmental Research Awards (PB), NCI R21 CA185536 (PB, JH, NW), Gulf Coast Consortium (PB, JH) CPRIT RP100969 and U54CA151668-03 (DGM) and NCI Cancer Center Support Grant CA016672.

## Author Contributions

N.W., J.H., J.S., M.C., E.C., N.M., D.M., C.M. and P.B. designed the study. N.W., J.H. and J.S. conducted the study. J.H. processed the data. N.W. and J.H. constructed the figures. N.W., J.H. and P.B. wrote the manuscript, and all authors contributed to the review and editing of the manuscript.

## Additional Information

**Supplementary information** accompanies this paper at <http://www.nature.com/srep>

**Competing financial interests:** The authors declare no competing financial interests.

**How to cite this article:** Whiting, N. *et al.* Real-Time MRI-Guided Catheter Tracking Using Hyperpolarized Silicon Particles. *Sci. Rep.* **5**, 12842; doi: 10.1038/srep12842 (2015).



This work is licensed under a Creative Commons Attribution 4.0 International License. The images or other third party material in this article are included in the article's Creative Commons license, unless indicated otherwise in the credit line; if the material is not included under the Creative Commons license, users will need to obtain permission from the license holder to reproduce the material. To view a copy of this license, visit <http://creativecommons.org/licenses/by/4.0/>

# Developing hyperpolarized silicon particles for advanced biomedical imaging applications

Nicholas Whiting<sup>a</sup>, Jingzhe Hu<sup>a,b</sup>, Pamela Constantinou<sup>c</sup>, Niki Zacharias Millward<sup>a</sup>, James Bankson<sup>d</sup>, David Gorenstein<sup>e</sup>, Anil Sood<sup>f</sup>, Daniel Carson<sup>c</sup>, Pratip Bhattacharya<sup>\*a</sup>

<sup>a</sup>Dept. of Cancer Systems Imaging, The University of Texas MD Anderson Cancer Center, 1515 Holcombe Blvd, Houston, TX USA 77030; <sup>b</sup>Dept. of Bioengineering, Rice University, 6100 Main St., Houston, TX USA 77005-1892; <sup>c</sup>Dept. of BioSciences, Rice University, 6100 Main St, Houston, TX USA 77005-1892; <sup>d</sup>Dept. of Imaging Physics, The University of Texas MD Anderson Cancer Center, 1515 Holcombe Blvd, Houston, TX USA 77030; <sup>e</sup>Dept. of NanoMedicine and Biomedical Engineering, The University of Texas Health Science Center at Houston, 7000 Fannin, Houston, TX USA 77030; <sup>f</sup>Dept. of Gynecologic Oncology and Reproductive Medicine, The University of Texas MD Anderson Cancer Center, 1515 Holcombe Blvd, Houston, TX USA 77030

## ABSTRACT

Silicon-based nanoparticles are ideally suited as biomedical imaging agents, due to their biocompatibility, biodegradability, and simple surface chemistry that is amenable to drug loading and targeting. A method of hyperpolarizing silicon particles using dynamic nuclear polarization (DNP), which increases magnetic resonance imaging (MRI) signals by 4-5 orders of magnitude through enhanced nuclear spin alignment, has recently been developed and shown viable as a contrast agent for *in vivo* MRI. Naturally occurring electronic defects on the particle surface obviate the need for exogenous radicals, and the enhanced spin polarization lasts for significantly longer than other hyperpolarized agents (tens of minutes, instead of <1 minute for other species). We report our recent advances in determining the MR characteristics of hyperpolarized silicon particles, which could lead to non-invasive, non-radioactive molecular targeted imaging of various cancer systems. A variety of particle sizes (20 nm-2  $\mu$ m) were found to have hyperpolarized relaxation times ranging from ~10-50 minutes. The addition of various functional groups to the particle surface, including biocompatible polymers, aptamers, and antibodies had no effect to the hyperpolarization dynamics or relaxation times, and appear to satisfactorily survive the harsh temperature conditions of DNP. Preliminary *in vivo* studies examined a variety of particle administration routes in mice, including intraperitoneal, tail vein, and rectal injections, as well as oral gavage. Ongoing experiments include targeted molecular imaging in orthotopic murine models of ovarian and colorectal cancers.

**Keywords:** Hyperpolarization, silicon particles, molecular imaging, nanomedicine, MRI

## 1. INTRODUCTION

### 1.1 Silicon particles

Shaped particles consisting of elemental silicon or silicon dioxide (silica) in the nanometer to micrometer size scale are receiving heightened interest for medical applications, including drug delivery and sensing<sup>1</sup>, due to their low cost and lack of toxicity for both the initial particles and their biodegradable downstream products<sup>2</sup>. Fluorescently-tagged silicon particles have been used to track living cells after uptake into the cytoplasm<sup>3</sup>, and commercially-available particles are being pursued for slow release drug delivery for the treatment of pancreatic cancer<sup>4</sup>. Because <sup>29</sup>Si (natural abundance: ~4.6%) is detectable using magnetic resonance imaging (MRI) or spectroscopy (MRS), developing silicon-based nanomaterials for MR studies may prove beneficial. <sup>29</sup>Si MRI would provide positive-contrast, background-free signals that are within the frequency range of most broadband clinical scanners capable of <sup>13</sup>C imaging. Silicon particles ranging in size, porosity, purity, and crystallinity are commercially available and cost-effective, and the field of silicon nanomaterials can benefit from developmental interests from the semiconductor industry. The simple surface chemistry of silicon particles is amenable to the addition of targeting agents and therapeutic drugs, furthering their application to the biomedical community.

\*pkbhattacharya@mdanderson.org; phone: 713-745-0769 fax: 713-563-4894

## 1.2 Hyperpolarized magnetic resonance

MRI and MRS measure the interactions of nuclear spins with radio waves inside of a strong magnetic field. Because most of the nuclear spins are oppositely aligned (due to the small energetic difference in nuclear spin levels), only a miniscule number of nuclei ( $10^{-5}$  to  $10^{-6}$ ) contribute to MR signals. Clinical MR studies focus  $^1\text{H}$  because it has the highest gyromagnetic ratio (providing more signal), near-unity isotopic abundance, and is highly prevalent in the physiology of living vertebrates. Most other MR-active species (including  $^{29}\text{Si}$ ) have orders-of-magnitude lower detection sensitivity compared to  $^1\text{H}$ , and therefore have not been extensively studied in a clinical setting. One way to overcome this drawback is through ‘hyperpolarization’ (HP), which refers to a collection of methods that temporarily boost MR signal intensities by redistributing the population of nuclear spins so that most occupy the same energy level—allowing the spins to constructively contribute to enhancing MR signals as opposed to destructively canceling each other. This process typically uses magnetic fields, low temperatures, and/or electromagnetic radiation to manipulate the spin population. Most hyperpolarization methods will highly spin-polarize an electron bath to near unity, then transfer this spin polarization to nearby nuclear spins through dipolar interactions. The result is an increase in detection sensitivity by 4-5 orders of magnitude, allowing the study of ‘non-conventional’ nuclei for molecular and metabolic imaging studies. Some of these include monitoring the metabolic conversion of HP  $^{13}\text{C}$  pyruvate to lactate and alanine to determine aerobic vs. anaerobic cellular metabolism<sup>5</sup> in the field of cancer detection, as well as void-space imaging using HP  $^3\text{He}$  and  $^{129}\text{Xe}$  in COPD and asthma patients<sup>6</sup>.

## 1.3 Dynamic nuclear polarization of silicon

A method of hyperpolarizing silicon micro- and nano-particles using solid-state dynamic nuclear polarization (DNP) has recently been developed and shown viable for *in vivo* imaging studies<sup>7</sup> in mice. In this method, low temperatures ( $<4\text{ K}$ ) and high magnetic fields ( $\sim 3\text{ T}$ ) are used to spin-polarize an ensemble of electrons. Then, this polarization is transferred to nearby nuclei through microwave-mediated dipolar spin-flips, taking advantage of the ‘solid effect’<sup>8</sup> route of DNP. This takes place on the surface of the silicon particles, which contain naturally-occurring oxidation defects. Because of this, the silicon particles do not require the addition of an exogenous radical source of free electrons<sup>9</sup>, which is needed for most other species polarized by DNP. The polarization is then spread throughout the particle via nuclear spin diffusion. Because the core of the particle protects the spins from exposure to depolarizing paramagnetic agents, the enhanced polarization is retained for tens of minutes, which is much longer than other hyperpolarized species, which lose their signal enhancement in tens of seconds<sup>10</sup> *in vivo*. This increased hyperpolarized retention time (HP  $T_1$ ) holds true even under physiological conditions, and creates an MR imaging window of approximately an hour, allowing the particles (once injected) the chance to transit to the physiological site of interest in a relevant timescale. Furthermore, the silicon particles, hyperpolarization process, and MRI/MRS in general are non-toxic and nonradioactive.

## 1.4 Purpose

We have previously demonstrated proof-of-concept *in vivo* imaging of silicon micro-particles in mouse models<sup>7</sup>. For this work, our goal was to further characterize and develop silicon particles that could be used for targeted molecular imaging of different cancer systems. This was accomplished by studying a variety of particle sizes (20 nm-  $2\mu\text{m}$ ), as well as adding different targeting groups to the silicon particle surface, such as antibodies and aptamers. We also examined whether surface functionalization negatively affected the hyperpolarization process (and *vice versa*), as well as attempted different relevant particle administration routes in orthotopic mouse models.

# 2. METHODS

## 2.1 Silicon particles

Different commercially-sourced silicon powders were either used as received (‘unfunctionalized’), or were coated in 3-aminopropyltriethoxysilane (APTES), then cross-linked with polyethylene glycol (PEG), an aptamer, or an antibody of choice for specific targeting. The bare particles ranged in size from 20 nm to  $2\mu\text{m}$ ; the smaller particles were mostly monocrystalline, while larger particles were polycrystalline/amorphous. For each sample, approximately 100 mg of silicon particles were packed into small Teflon tubes (5 mm ID x 2 cm length) normally used as inserts for electron paramagnetic resonance experiments, which are microwave-invisible and withstand the cryogenic temperatures of DNP.

## 2.2 Solid-state dynamic nuclear polarizer

The sample tubes were then inserted into the home-built solid-state DNP polarizer (Figure 1), which consists of a superconducting magnet (~2.9 T), helium flow cryostat (~3 K), and microwave source (~100 mW) that was frequency-modulated from 80.83 to 80.90 GHz to cover a wider portion of the silicon ESR line. The microwaves were directed to the sample tube using a waveguide and slot antenna. The sample also resides within an *in situ* NMR coil, allowing quality assurance using a miniature NMR spectrometer. *In situ* NMR studies to monitor the buildup of  $^{29}\text{Si}$  signal during DNP used a saturation recovery pulse sequence. After sufficient polarization time (1-17 hours), the sample tube is quickly removed, warmed to room temperature, and transported to the MRI scanner suite for imaging studies ( $T_{\text{transport}} < 1$  minute).

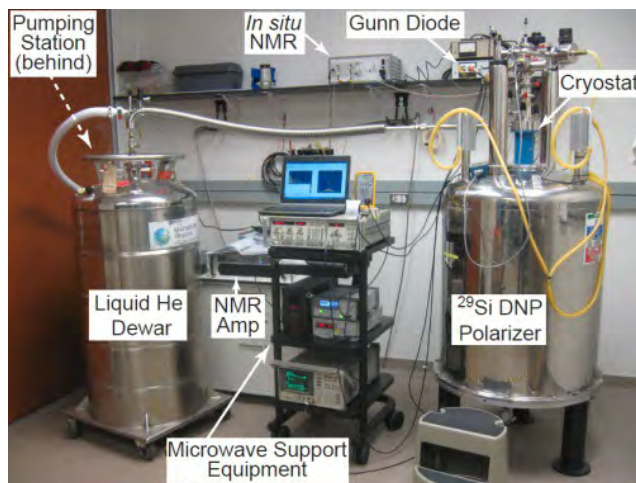


Figure 1: Labelled picture of home-built solid-state DNP device for  $^{29}\text{Si}$  hyperpolarization. The magnetic field is supplied by a superconducting magnet, while a liquid helium flow cryostat allows the sample to be held at cryogenic temperatures. The Gunn diode provides microwaves to transfer polarization from electrons to nearby nuclei, and the on-board NMR system allows the process to be monitored in real time.

## 2.3 Imaging protocol

All imaging experiments were performed on a 7 T horizontal-bore small animal MRI scanner using either a dual-tuned  $^1\text{H}/^{29}\text{Si}$  litz coil for co-registered imaging (35 mm ID; homogenous rf region ~52 mm along  $z$ -axis) or a dual-coil set-up consisting of a home-built  $^{29}\text{Si}$  surface coil (38 mm) and commercial  $^1\text{H}$  volume coil. A small aliquot of silicon oil was used for calibration purposes; achievable  $^{29}\text{Si}$  nuclear spin polarization values were typically on the order of 1%. Spectroscopy was performed using a simple pulse/acquire sequence. Imaging studies of solid-state particles, dissolved particles in phantoms, and *in vivo* mouse models used a variable tipping angle Rapid Acquisition with Refocused Echoes (RARE) sequence. Image reconstruction and post-processing was performed in MatLab. For dissolution studies, particles are suspended in phosphate buffered saline and administered to the phantom or mouse model.

## 2.4 Animal handling

All animal studies were performed in accordance with the UT MD Anderson Cancer Center IACUC. Mice were placed on an MR-compatible heated sled and anesthetized with 2% isoflurane (in 0.75 l/min oxygen) administered via nose cone. Dissolved particles were administered to the mice using different methods, including intraperitoneal injection, oral gavage, tail vein injection, or administered through the rectum.

# 3. RESULTS

## 3.1 Effects of particles size

A number of different silicon particle sizes were evaluated, ranging from 20 nm to 2  $\mu\text{m}$  average mean diameter. The time needed to reach steady-state nuclear spin polarization was dependent on particle size due to nuclear spin diffusion spread throughout the particle. Smaller nanoparticles (<100 nm) only required one hour of DNP time to reach steady-

state polarization levels, while larger microparticles needed more than 10 hours (Figure 2). Furthermore, when adjusted for mass, a dependence on the overall  $^{29}\text{Si}$  NMR signal intensity vs. particle size was noticed. This is likely due to one or both of the following scenarios: (a) differences in the number and position of electronic defects as a function of particle size and crystallinity; and (b) differences in surface-to-volume ratio between particle sizes (polarization is quickly depleted on the surface, while spins in the particle core are relatively protected). Because of this significant difference in attainable signal intensities, only larger particles (2  $\mu\text{m}$ ) have been able to be studied for *in vivo* applications. Current studies are focused on altering the surface defects of smaller nanoparticles (<100 nm) to improve signal enhancement

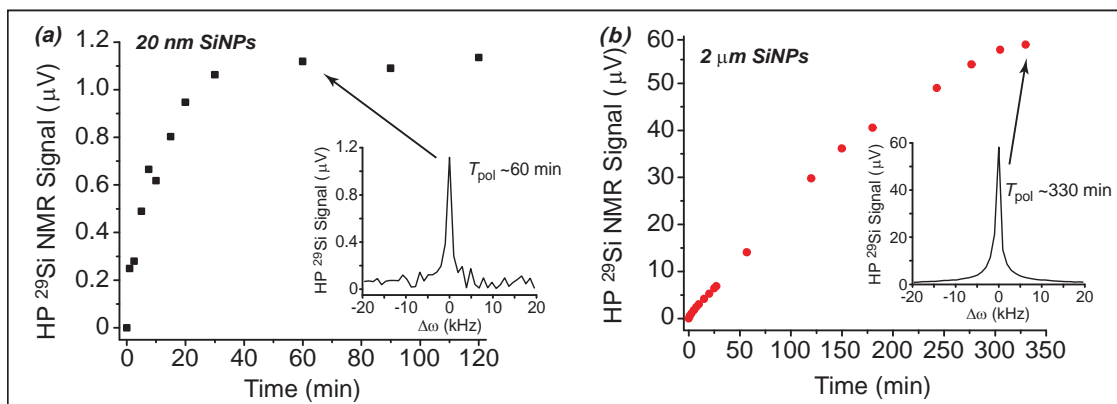


Figure 2:  $^{29}\text{Si}$  polarization buildup curves for (a) 20 nm and (b) 2  $\mu\text{m}$  size particles. *Insets*: example NMR spectra at relevant time points. Data was collected in real time during DNP process using on-board NMR system and pulse/acquire sequence.

levels. Because the primary means of depolarization (hence, signal loss) is through nuclear spin diffusion from the core back to the surface, the hyperpolarization relaxation time also varies on the particle size, with smaller particles losing their enhanced signal at a faster rate than larger particles due to the decreased distance from the surface to the core (Table 1).

Table 1:  $^{29}\text{Si}$  polarization decay times for different silicon nanoparticle (SiNP) sizes, surface chemistries, and time spent in the DNP device. Particles of 2  $\mu\text{m}$  size are shown with normal surface chemistry, as well as the addition of polyethylene glycol (PEG) and an E-selectin thioaptamer (ESTA-1).

<b><math>^{29}\text{Si}</math> Hyperpolarization Decay Times</b>		
SiNP size	HP $T_1$	DNP time
20 nm	~10 min	~80 min
30 nm	~17 min	~120 min
70 nm	~16 min	~60 min
2000 nm	~62 min	~300 min
2000 nm PEGylated	~55 min	~330 min
2000 nm ESTA-1	~56 min	~300 min

### 3.2 Effects of surface chemistry

To further develop these particles as targeted molecular imaging agents, the ability to add functional groups to the particles' surfaces, as well as the effects of these altered surface chemistries, were studied. Particles were functionalized with polyethylene glycol to improve hydrostability and biocompatibility. Indeed, the PEGylated particles exhibited improved dissolution characteristics when compared to bare silicon particles. ESTA-1, a thiophosphate-modified oligonucleotide aptamer<sup>11,12</sup> that seeks out E-selectin—a glycoprotein that is overexpressed on the endothelial cell surface of certain ovarian cancer tissue—was also added to the silicon particles (Figure 3).

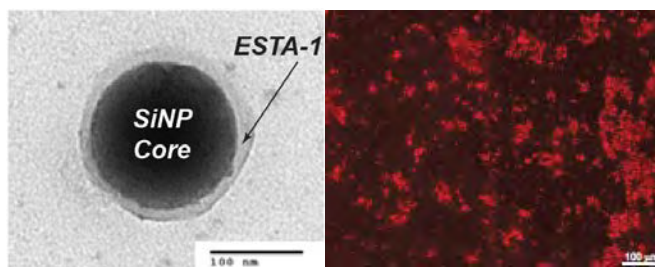


Figure 3: E-selectin thioaptamer functionalized silicon particles. (a) Scanning electron micrograph (SEM) of an ESTA-1 nanoparticle. (b) Fluorescent micrograph of optically-tagged (Cy3) ESTA-1 silicon particles, showing successful coupling of the aptamer and the silicon particles.

E-selectin is not present in normal tissue, making it a potentially useful biomarker for ovarian cancer. On their own, the thioaptamers bind to E-selectin with nanomolar affinity, and are minimally cross-reactive with other selectins. They have also been demonstrated to bind to cultured endothelial cells and tumor-associated vasculature in murine and human carcinomas<sup>12</sup>. In addition to the high levels of affinity and specificity, thioaptamers are easily synthesized and conjugated, and are biocompatible and resistant to nuclease. These ESTA-1 functionalized particles were tagged with a fluorescent dye (Cy3) to allow cross-correlation between MRI and optical imaging studies. Hyperpolarization of these functionalized particles did not show any ill effects to the hyperpolarization level or relaxation rate, despite changes to the surface chemistry (Figure 4). This is an important step in the progression of these particles as targeted imaging agents. Ongoing studies include injecting ESTA-1 silicon particles into orthotopic ovarian cancer mouse models to test their ability to function as targeted imaging agents. Particles that were functionalized with an anti-MUC1 antibody (to target mucin overexpression in colorectal cancer<sup>13</sup>) and then exposed to the harsh temperature conditions of DNP were afterwards shown to retain their structure and ability to target mucin *in vitro*.

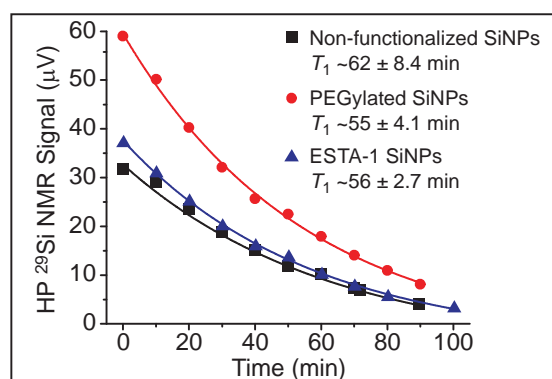


Figure 4: <sup>29</sup>Si polarization decay curves for 2 μm sized silicon particles with different surface chemistries. The PEGylated particles (red circles) have an initially higher <sup>29</sup>Si signal intensity due to a larger sample mass.

### 3.3 Initial imaging studies

Following DNP, the sample can be efficiently transferred to the small animal MRI scanner without a significant loss of polarization. Compared to previous studies<sup>7</sup> at a different location using the same experimental parameters, the 7 T scanner in this study provides nearly an order of magnitude improvement in SNR due to improved electromagnetic shielding properties. Because the benefits of the hyperpolarization process are field-independent, the increase in field strength was largely inconsequential. Initial imaging scans using the silicon particles in their sample tube as a phantom reveal that the signal is still observable 30 minutes after completion of the DNP process (Figure 5). Most other hyperpolarized species, including <sup>13</sup>C-pyruvate, have much shorter relaxation times under ambient conditions (~1 minute). This increased relaxation time will allow the silicon particles the opportunity to transit to their targeted site *in vivo* in a relevant timeframe.

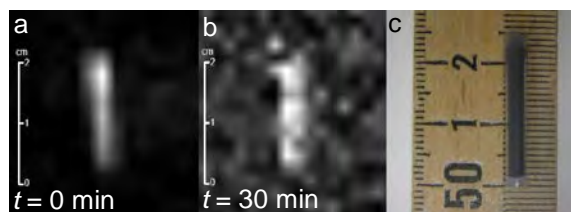


Figure 5: Initial MRI of silicon particles inside sample tube. (a)  $10^\circ$  RARE sequence immediately after 4 hours of DNP. (b)  $90^\circ$  RARE sequence 30 minutes after DNP. (c) Photo of silicon particles in sample tube/phantom (particle region: 2 cm long; 5 mm diameter).  $\sim 100$  mg of unfunctionalized  $2 \mu\text{m}$  silicon particles were used for this study.

Following the successful phantom imaging, we turned towards proof-of-concept studies in mouse models to demonstrate the long-lasting hyperpolarized  $^{29}\text{Si}$  signal, which was still detectable 30 minutes after intraperitoneal injection (Figure 6).

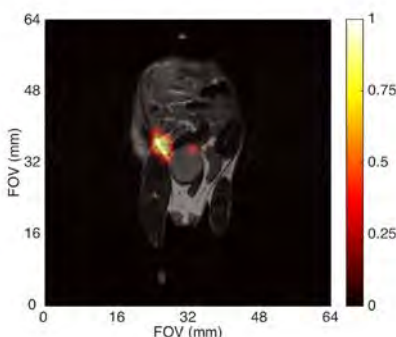


Figure 6: Long-lasting  $^{29}\text{Si}$  signal *in vivo* for  $\sim 100$  mg of hyperpolarized silicon particles ( $2 \mu\text{m}$  diameter) 30 minutes after intraperitoneal injection.  $^{29}\text{Si}$  signal (color) co-registered with  $^1\text{H}$  anatomical coronal scan (greyscale); each scan used a  $90^\circ$  RARE imaging sequence for the respective nuclei. Processed  $^{29}\text{Si}$  signal used 35% threshold to filter background. Most  $^{29}\text{Si}$  signal at this timepoint is from the largest particles, which gravitationally settle at the injection site.

### 3.4 Silicon particle administration routes

Because different orthotopic cancer systems will have different locations throughout the body, and the optimal delivery of the targeted particles is needed to maximize the chances of success, a variety of different methods for suspending the particles in buffer and administering them to mouse models have been tested. It was found that the dissolution process works best in the fringe field of the 7 T MRI scanner, where the field is strong (compared to Earth's field) and the chance of zero-field crossing is minimized. We have administered the particles to mouse models in a variety of ways; these include: injecting into the intraperitoneal (IP) cavity, tail vein, and into the large intestines via the rectum, as well as through oral gavage. Tail vein injection, which is the most common method of administering MR contrast agents to mouse models, was shown to not be viable for the  $2 \mu\text{m}$  sized particles due to their large size and relative insolubility, despite PEGylation. Particles would travel approximately 1 cm up the tail vein before stopping due to a clog. Also, the viscosity of the nanoparticle suspension requires the use of a smaller gauge needle that is not conducive to tail vein injections. This particle injection method will be revisited once we shift to using smaller particles for *in vivo* studies.

The other administration routes were more successful, and *in vivo* hyperpolarized signal was achieved for all of them (Figure 7). Oral gavage, which can be used to study the upper gastrointestinal (GI) tract, was difficult to administer in a timely fashion using a soft plastic application needle (due to proximity to MRI scanner) and while keeping the mouse stationed on the sled. However, we were able to achieve images of the particles inside the stomach using this method (Figure 7a). Injecting through the rectum (Figure 7b), to study diseases of the large intestines, was achieved through insertion of a soft, flexible applicator or small diameter ( $\sim 1/8''$ ) rubber tube. This method kept the particle concentration per voxel high (as the particles are contained in a smaller volume), leading to increased  $^{29}\text{Si}$  signal. This method works

best when used in conjunction of administering an enema at least 30 minutes prior to inserting the particles. Additional gains may be made when adding food restrictions and laxatives the night prior to the scan. We do note that fecal blockages can be problematic with this administration route, but have imaged particles up to the cecum. IP injections (Figure 7c), which can be used for targeting orthotopic ovarian cancer, displayed sufficient  $^{29}\text{Si}$  signal post-injection. However, especially at later time points, the majority of the signal was concentrated at the injection site, meaning that the large microparticles are not dispersing throughout the cavity. Physical manipulation of the mouse post-injection resulted in a movement of the  $^{29}\text{Si}$  signal, but is not considered active targeting. It is thought that the large size of the microparticles prevents them from actively transiting throughout the IP cavity; instead, they gravitationally settle at the injection site. Ongoing studies are attempting to use distension of the IP cavity to encourage dispersion; additional studies will use smaller  $^{29}\text{Si}$  nanoparticles for *in vivo* studies. We are also currently exploring direct intratumoral injection of targeted particles in cancer mouse models.

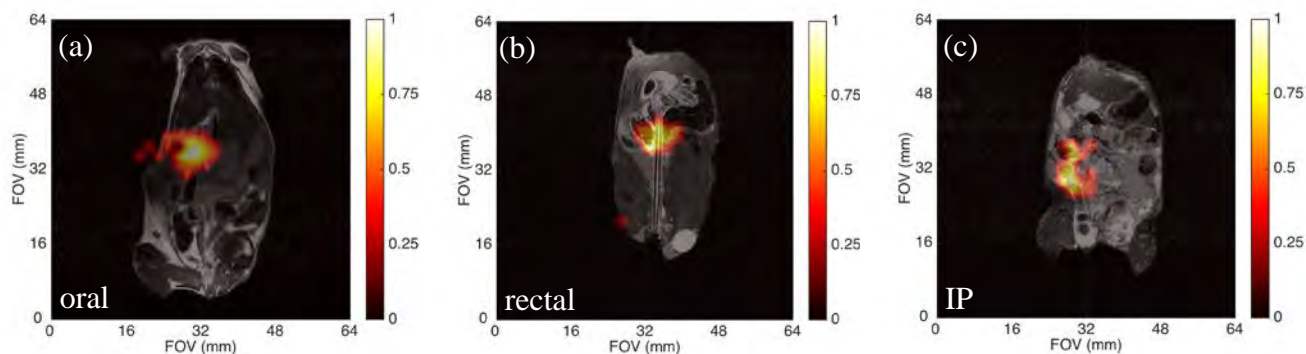


Figure 7: *In vivo*  $^{29}\text{Si}$  MRI for 2  $\mu\text{m}$  PEGylated silicon particles. (a) Administration of silicon particles via oral gavage, followed by a 5 minute wait and  $90^\circ$  RARE imaging sequence. Image reconstructed with 35% threshold. (b) Administration of silicon particles via injection through the rectum using a soft tube, followed by a 5 minute wait and a  $90^\circ$  RARE sequence, with 35% threshold for image reconstruction. (c) Administration of silicon particles via intraperitoneal injection followed by a 10 minute wait and  $90^\circ$  RARE sequence, with 40% threshold. Silicon images (*color*) are co-registered with  $^1\text{H}$  coronal slice anatomical images (*greyscale*) acquired with  $^1\text{H}$   $90^\circ$  RARE scan.

#### 4. CONCLUSIONS

In this work, we have demonstrated the hyperpolarization of a variety of different silicon particle sizes and surface chemistries. The larger microparticles provided the highest signal enhancements over the longest time durations, likely due to their polycrystalline/amorphous structure and smaller surface-to-volume ratio when compared to smaller particles. The addition of targeting groups to the particles' surface did not alter the hyperpolarization dynamics, and functional groups were shown to survive the harsh conditions of DNP. High field imaging was accomplished using phantoms and mouse models via a variety of particle administration methods. These results show a promising future for hyperpolarized silicon particles to serve as non-invasive molecular imaging agents. However, work is still needed; ongoing studies involve developing small, more physiologically-relevant nanoparticles for *in vivo* imaging and continuing with the targeted imaging studies in orthotopic mouse models.

#### REFERENCES

- [1] Tasciotti, E., *et al.* "Mesoporous Silicon Particles as a Multistage Delivery System for Imaging and Therapeutic Applications". *Nature Nanotechnology* **3** (2008).
- [2] Park, J.-H., *et al.* "Biodegradable luminescent porous silicon nanoparticles for *in vivo* applications". *Nature Materials* **8**, 331-336 (2009).
- [3] Osminkina, L.A., *et al.* "Photoluminescent biocompatible silicon nanoparticles for cancer theranostic applications". *Journal of Biophotonics* **3**(2012).

- [4] Corp, p. <<http://www.psivida.com/products.html>>, 2012).
- [5] Golman, K., Zandt, R., Lerche, M.H., Pehrson, J. & Ardenkjaer-Larsen, J.H. "Metabolic Imaging by Hyperpolarized  $^{13}\text{C}$  Magnetic Resonance Imaging for In Vivo Tumor Diagnosis". *Cancer Research* **66**, 10855-10860 (2006).
- [6] Fain, S.B., *et al.* "Functional lung imaging using hyperpolarized gas MRI". *Journal of Magnetic Resonance Imaging* **25**, 910-923 (2007).
- [7] Cassidy, M., Chan, H.R., Ross, B.D., Bhattacharya, P.K. & Marcus, C.M. "In Vivo Magnetic Resonance Imaging of Hyperpolarized Silicon Nanoparticles". *Nature Nanotechnology* **8**, 363-368 (2013).
- [8] Dementyev, A.E., Cory, D.G. & Ramanathan, C. Dynamic Nuclear Polarization in Silicon Microparticles. *Physical Review Letters* **100**, 127601 (2008).
- [9] Cassidy, M., Ramanathan, C., Cory, D.G., Ager, J.W. & Marcus, C.M. "Radical-free dynamic nuclear polarization using electronic defects in silicon". *Physical Review B* **87**, 161306(R) (2013).
- [10] Aptekar, J.W., *et al.* "Silicon Nanoparticles as Hyperpolarized Magnetic Resonance Imaging Agents". *ACS Nano* **3**, 4003-4008 (2009).
- [11] Mann, A.P., *et al.* "Identification of Thioaptamer Ligand against E-Selectin: Potential Application for Inflamed Vasculature Targeting". *PlosOne* **5**, 13050 (2010).
- [12] Mann, A.P., *et al.* "E-Selectin-Targeted Porous Silicon Particle for Nanoparticle Delivery to the Bone Marrow". *Advanced Materials* **23**, H278-H282 (2011).
- [13] Nakamura, H., *et al.* "Detection of circulating anti-MUC1 mucin core protein antibodies in patients with colorectal cancer". *Journal of Gastroenterology* **33**, 354-361 (1998).